Reflection and transmission coefficients in fluid-saturated poroelastic sediments

Fabien Borocin

Thesis submitted for the degree of Master of Philosophy

School of Geosciences

University of Edinburgh

December 2003

Abstract

The interpretation of reflection, transmission and conversion (RTC) coefficients in fluid-saturated porous rock is of utmost importance for the characterisation of hydrocarbon reservoirs. It has also been suggested that high-pressure pore-fluid is responsible for anomalously high (up to 0.15-0.25) values of reflection coefficients (deep crustal reflectors) in the lower crust, subduction zones and subglacial deforming sediments. In my thesis I consider the interaction of seismic waves at the interface between fluid-saturated poroelastic media, taking properly into account the effects of fluid-solid interaction.

I reproduce dynamic equations for wave propagation in poro-elastic media and obtain an explicit wave decomposition in up- and down-going wave components. I then develop an algorithm to compute RTC coefficients at the interface between two arbitrary poro-elastic media, when possible pore-pressure discontinuity at the interface is taken into account.

My algorithm is written in a matrix form allowing me to compute RTC coefficients for plane waves at all frequencies and all angles of incidence. This algorithm encompasses both visco-elastic and poro-elastic cases including the effects caused by partially sealed interface.

Using numerical examples I show that my algorithm is consistent with (visco-)elastic case. It is designed in a matrix form suitable for conventional computations of multilayered stacks as used in the reflectivity method. A range of possible applications and extensions such as wave propagation in finely-layered fluid-saturated sediments are discussed.

Declaration

I hereby declare that this thesis has been composed by myself and that the work described is entirely my own unless explicitly stated in the text.

Fabien Borocin

Software used for this thesis:

This thesis was written using LaTeX . Figures were drawn by Matlab from programs which were written by myself in Fortran and Matlab scripts.

Acknowledgements

I thank Prof. Ian Main and Dr Sergei Zatsepin of Edinburgh University without whose inputs this thesis would not be what it is and Dr Enru Liu and Dr Mark Chapman of the British Geological Survey (BGS) for a stimulating and friendly environment. It is most of all Sergei's scientific guidance and extreme patience which made this work come to fruition. It is published with the approval of the executive director of the BGS and with financial support from LB Consulting and from the sponsors of the Edinburgh Anisotropy Project of the BGS.

Special thanks go to my parents, sister and godparents for their love and support.

Contents

Abstract i

Declaration ii

Acknowledgements iii

Table of Notations 1

1 INTRODUCTION 3

1.1 General review 3

1.2 A short history of Biot slow wave 5

1.3 Thesis plan 8

2 WAVE EQUATIONS IN FLUID-SATURATED SEDIMENTS 9

2.1 Introduction 9

2.2 Dynamic poroelastic equations 10

2.3 Constitutive relationships for fluid-saturated porous rock 11

2.4 Wave equations for compressional waves 11

2.5 Wave equation for shear wave 12

2.6 Physical meaning of Biot parameters 13

2.7 Summary 14

3 DISPERSION EQUATIONS 15

3.1 Introduction 15

3.2 Dispersion equations for P-wave and Biot slow wave 16

3.3 Dispersion equation for S-wave 18

3.4 Numerical results for dispersion equations 19
3.5 Summary 21

4 PLANE WAVE DECOMPOSITION **22**
4.1 Introduction 22
4.2 Compressional wave components 23
4.3 Shear wave components 24
4.4 Final results 26
4.5 Wave energy flux 28
4.6 Summary 28

5 REFLECTIONS AND TRANSMISSIONS IN POROELASTICITY **29**
5.1 Introduction 29
5.2 Boundary conditions 30
5.3 S_H wave 31
5.4 Reflection matrix for P-, S-, Biot waves 35
5.5 Summary 40

6 NUMERICAL ALGORITHM **41**
6.1 Introduction 41
6.2 Viscoelastic approximation 42
6.3 Summary 47

7 POROELASTIC CASE **48**
7.1 Introduction 48
7.2 Poroelastic effects at different frequencies. 48
7.3 Summary 58

8 APPLICATION TO OCEAN-BOTTOM SEDIMENTS **59**
8.1 Introduction 59
8.2 Numerical results 60
8.3 Summary 66

9 CONCLUSION **67**

References **70**

Table of Notations

υ displacement of solid frame,

ν relative displacement of fluid to frame,

e dilatation of the element attached to the frame,

ξ increment of fluid content,

ρ total density,

ρ_r grain density,

ρ_f density of fluid,

c tortuosity,

ϕ porosity,

a pore size,

η the fluid viscosity,

k permeability,

k_s surface permeability,

p_f fluid pore pressure,

σ stress,

W strain energy,

K_b bulk modulus of the skeleton frame,

K_r indivdual grain bulk modulus,

K_f fluid bulk modulus,

μ shear modulus of the frame,

δ log decrement,

q horizontal slowness,

p ratio of vertical over horizontal slowness for P-wave,

b ratio of vertical over horizontal slowness for $Biot$-wave,

s ratio of vertical over horizontal slowness for S_V-wave,

z ratio of vertical over horizontal slowness for S_H-wave,

ς total slowness,

X square of slowness,

R scalar factor relating colinear displacement of fluid to displacement of frame,

R matrix of reflection/transmission coefficients for amplitudes,

E average energy flux in the direction of wave propagation.

Chapter 1

INTRODUCTION

1.1 General review

A general feature of sedimentary rocks is that they are layered and heterogeneous at many scales. Characterizing the heterogeneities and their scales is currently one of the major problems in reservoir characterization. The virtually unsolvable problem of seismic wave propagation in such a complicated physical structure is normally substituted with the much more tractable problem of seismic wave propagation in some effectively homogeneous medium where the effects of attenuation, dispersion and effective anisotropy account for complex inhomogeneous structure at different scales.

The attenuation of seismic waves can be due to the anelastic loss of energy caused by local absorption in the medium of purely elastic scattering of seismic waves at heterogeneities. Multiple scattering and diffraction disperse seismic waves in all directions, particularly when heterogeneities are of similar size to the seismic wavelength. Frequency dependence of attenuation and scattering inevitably results in the dispersion of seismic waves.

In two and three dimensions, dispersion is introduced by a path effect known as the Wielandt effect [Mukerji et al. 1995]: as the wavelength shortens, waves tend to find fast paths and diffract around slower inhomogeneities. In the long wavelength limit however, the wave does not see the inhomogeneities individually but catches some spatially averaged properties: we therefore have an effective homogeneous medium. When a heterogeneous structure has some preferable directions of orientation at the microscopic scale, the equivalent macroscopically homogeneous medium will be effectively anisotropic. This averaging process is performed with the help of methods from effective medium theory [de la Cruz and Spanos 1985, Hudson and Knopoff 1989].

Effective attenuation of seismic waves is a more complicated and still unresolved problem. At the pore scale we may have different mechanisms contributing to the loss of elastic energy of propagating seismic waves. Attenuation can be caused by microscale viscous fluid flow, capillary forces in pore throats and squirt flow caused by local fluid exchange between heterogeneous inclusions with different compressibilites [Bourbie et al. 1986]. When modelling seismic waves the character of attenuation strongly depends on the selected physical mechanism. However some rigorous relationships between the real and imaginary part of the complex refractive index effectively linking dispersion and attenuation can be established from the principle of causality [Futtermann 1962].

More recently, O'Donnell et al. (1978) considered the complex susceptibility and obtained a pair of simple relationships connecting dispersion and attenuation, which were verified experimentally by Lee et al. (1990). However, these relations hold only for the component of dispersion induced by attenuation. While attenuation always brings dispersion, we can have dispersion occuring with no attenuation (wave guide for instance).

A finely layered sediment consisting of isotropic thin layers will behave at a large wavelength like an equivalent anisotropic (transversely isotropic) medium. According to Helbig [1984] we effectively replace three rapidly fluctuating parameters (rock density and P- and S-velocities) with a larger number of smoothly varying parameters characterising effective anisotropy.

The way in which layering affects wave propagation depends on the ratio of wavelength to layer spacing. When seismic wavelength is much smaller than typical layer thickness, propagation of seismic waves can be modelled using ray theory methods [Aki and Richards 1981]. In the opposite limit when wavelength is much greater than layer thickness, waves propagate in an equivalently anisotropic medium. Some experimental work gives a value of ten [Mukerji et al., 1995], numerical simulations give values between five and eight depending on the constituents of the layers [Carcione et al., 1991], and physical arguments make up a value of three [Helbig 1984].

As was shown by Backus [1962], a set of fine isotropic layers whose spacings are far smaller than the wavelength is equivalent to one anisotropic layer. Using a group-theory framework, Schoenberg and Muir [1989] generalized this result to a set of layers with arbitrary anisotropies. An exact result in the static limit, it was extended to a broader long wavelength range by Folstad and Schoenberg [1995] who introduced a frequency dependence. This is justified experimentally by the work of Sams [1995] who shows that fine layering below the resolution of a sonic logging will appear as induced dispersion and anisotropy.

It was understood by White et al. [1975] that fluid flow induced by propagating seismic waves at the interface affects strongly the transmissivity of fine-layered sediments. In the next section I present a short review of fluid-related phenomena in layered porous sediments.

1.2 A short history of Biot slow wave

Despite the fact that poroelastic constitutive relationships had been widely used by engineers in applications to soil mechanics problems for more than one century, only in 1951 was the first application of poroelasticity for the problem of seismic wave propagation initiated by F. Gassmann. Gassmann derived rigorous relationship between bulk modulus of fluid-saturated porous rock and bulk modulus of its dry skeleton. This relationship depends on bulk modulus of mineral grains constituting sedimentary rock and fluid bulk modulus. It is difficult to overestimate the consequences Gassmann's result had on seismic exploration development in the second half of the twentieth century. However, Gassmann's relationship was valid only for very low seismic frequencies, inhibiting testing Gassmann's prediction in laboratory experiments where acoustic frequency is very high ($\approx 0.5MHz$). The dynamic theory of wave propagation in fluid-saturated (poro-elastic) rock was developed by Maurice Biot [1956, 1962]. Biot's theory predicted an additional frequency-dependent attenuation caused by pore-fluid flow induced by propagating seismic waves. Another unexpected prediction of Biot's theory was the existence of a second (slow) compressional wave. The existence of this slow (Biot) compressional wave was later confirmed in the laboratory experiment [Plona 1980]. Unfortunately Biot's wave equation contained a large number of poorly defined parameters with obscure physical meaning. The physical meaning of Biot's parameters was established by Geertsma and Smit [1961]. They also demonstrated that in the low frequency limit Biot's equations reduce to Gassmann's relationship.

A significant deviation of Biot's results from Gassmann's relationship occurs at the characteristic (Biot-) frequency

$$\omega_B = \frac{\phi\eta}{\rho_f\kappa} \tag{1.1}$$

where ϕ and κ are the porosity and specific permeability of rock and ρ_f and η are the density and viscosity of fluid. Thompson et al. [1987] inferred this characteristic or relaxation frequency for fifty sandstones with a range of permeability that spanned over seven orders of magnitude. They had shown that this frequency lies in the range $10KHz < \omega_B/2\pi < 10^4KHz$ which makes

the difference between Biot's and Gassmann's results insignificant in the seismic frequency band. Later on Dvorkin and Nur [1993] demonstrated that another attenuation mechanism caused by pore-fluid flow at the microscale level (squirt flow) interferes with Biot's mechanism, making Biot's attenuation rather irrelevant for the problem of elastic wave propagation in sedimentary rock. However, Geertsma and Smit [1961] pointed out that the second (slow) compressional wave (also called *B*iot wave) can affect the reflection coefficients at the boundary between fluid-saturated porous medium and elastic solid or liquid. In a series of papers, Deresiewicz and Rice [1962, 1964] thoroughly investigated the influence of compressional wave of second kind on reflection and transmission coefficients of conventional P-wave for a variety of interfaces (considering an interface between fluid-saturated porous half-space and solid, liquid or free half-space). However, their results were limited to the case of P-wave with normal incidence. Hajra and Mukhopadhyay [1982] and Stoll [1989] have followed Deresiewicz and Rice's [1962, 1964] approach to investigate reflection coefficients at oblique incidence respectively from an elastic solid and from a liquid to a porous medium. As an additional result they indicated a possible important influence of Biot wave on the dispersion characteristics of Stoneley waves.

Rosenbaum [1974] applied Biot's theory to a numerical study of sound pulses propagating in a cylindrical borehole and along plane interface. He found that the value of permeability coefficient affects the attenuation of the signal. He demonstrated that for the plane interface the effect on the P-arrival is relatively small, on the S-arrival moderate and on the Stoneley wave it is large, but only when source and detector are close to the interface. Similar conclusions hold for the well-logging tool in the borehole. Another application of Biot's equation is due to Stoll [1977, 1989] who applied Biot theory to the acoustic model of unconsolidated sea-floor sediments. He reformulated Biot's theory and explicitly identified physical parameters convenient for unconsolidated sediment description. He applied his model to study velocity, attenuation and reflection in ocean sediments.

In the '80s and '90s the development of Biot's theory went along two mainstreams. First, extensive research was undertaken to derive Biot's equations from microstructural approach [Levy and Sanchez-Palencia 1977, de Vries 1989]. The main objective was to identify Biot's parameters with real petrophysical properties of sedimentary rock. Unfortunately, this frequently resulted in introducing even greater number of petrophysical microstructural parameters. In general, all derived wave equations were consistent, if not identical to Biot's wave equations for all practical purposes. One interesting result is the theoretical possibility of existence of the second S-wave [de la Cruz & Spanos, 1985].

An essentially more important and far reaching application of Biot's theory concerned the problem of dispersion of seismic waves in fine-layered medium. This research can be roughly subdivided in two main directions. The first is related to possible influence of wave-induced fluid flow (Biot wave) on seismic anisotropy of fine-layered sediments. The second direction of research is related to the consequences of wave-induced fluid-flow between thin layers on the dispersion and attenuation of seismic waves.

In 1971 O'Doherty and Anstey had shown how multiple scattering in thin layers effects the transmissivity of seismic pulses through the sequence of fine-layered sediments. This paper has greatly advanced understanding of the physics of seismic primaries. O'Doherty and Anstey [1971] found a very elegant way to describe this effect.

It was understood by White et al. [1975] that wave-induced fluid exchange between thin layers could have a strong influence on this stratigraphic filtering. When P-wave wavelength is larger than the layer thickness it will compress several layers simultaneously. Because of different compressibilities of layers, wave-induced fluid pressure will be different in adjacent layers. The consequent equilibration of the induced-fluid pressure by viscous flow between layers will result to the significant loss of energy and consequently to the attenuation of P-wave. The maximum of this attenuation occurs at some characteristic frequency when the fluid pressure diffusion length (or Biot slow-wave wavelength) is of the order of characteristic frequency of typical layer spacing. This characteristic frequency

$$\omega_c = \frac{K_f \kappa}{\eta \phi d^2} \tag{1.2}$$

where K_f, the bulk modulus of fluid, is inversely proportional to the square of typical layer thickness d. For sufficiently thin layers with a thickness of several meters and for permeability value around a decidarcy, frequency ω_c falls in the seismic frequency band. White et al. [1975] modelled this low frequency attenuation caused by Biot slow-wave between alternating layers neglecting scattering effects. Gurevitch and Lopatnikov [1995] extended the analysis of White et al. [1975] for the case of randomly layered sediments. They received analytical results for the attenuation and dispersion caused by Biot slow-waves induced at the interface in the single scattering approximation, assuming that physical properties contrasts between individual layers are small. Gelinsky and Shapiro [1997] extended previous analysis of P-waves in randomly layered sediments taking into account multiple P-wave scattering. All the results mentioned above were limited to plane P-wave at normal incidence (i.e. one-dimensional case).

1.3 Thesis plan

My main objective is to develop a reliable algorithm for plane wave decomposition and computation of reflection, transmission and conversion coefficients in fluid filled poroelastic medium. I will start by writing in chapter 2 the linear dynamic equations of motions and reproducing the constitutive equations for an isotropic poroelastic medium. From the equations of motion, I derive in chapter 3 the dispersion equations from which I obtain the complex slownesses as an explicit function of frequency. I go on to provide some numerical results showing the dispersion effect on seismic velocities in poroelastic medium.

Chapter 4 is the most important chapter in my thesis. In this chapter I derive the decomposition of a seismic wave-field into downgoing and upgoing harmonic components for all waves (P, Biot, S_V, and S_H waves) involved in the propagation of seismic waves in poroelastic medium. In the decomposition of poroelastic wave field into different wave components I follow closely the approach developed by David Taylor [1997]. The main result is the complete table of these wave-field components as a function of horizontal slowness for an arbitrary frequency. I also provide energy flux expressions for different wave-field components.

In chapter 5 I derive a matrix equation for reflection/transmission/conversion coefficients at the interface between two arbitrary poroelastic media. I discuss different approaches to the problem of boundary conditions between two fluid-saturated porous solids. I conclude that the boundary conditions of Deresiewicz and Skalak [1963] are the most general and consistent boundary conditions in the theory of poroelasticity. As a simple illustration of my approach I provide results for reflection and transmission coefficients for S_H waves which are decoupled from P, Biot, and S_V wave-field.

In chapter 7 I apply my algorithm to the general case of the interface between two poroelastic media with different but relatively high characteristic Biot frequencies. I specifically choose the most complicated case when two critical angles are present for an incident S-wave. I show that there is a significant influence of Biot wave on the reflection of P- and S-wave in the vicinity of critical angles.

In chapter 8 I apply my algorithm to the realisitic case of interface between two layers of ocean-bottom sediments. High porosity and permeability of unconsolidated ocean-bottom sediments result in pronounced effect of Biot wave on reflection and transmission of incident P-wave-field. As an additional result I show the dependence of reflection, transmission and conversion coefficients for energy fluxes.

Chapter 2

WAVE EQUATIONS IN FLUID-SATURATED SEDIMENTS

2.1 Introduction

My main objective in this chapter is to obtain wave equations for seismic waves in fluid-saturated poroelastic medium. I start from the equations of motion for a two-phased system consisting of elastic frame filled with viscous fluid. Following Maurice Biot [1956] approach I introduce constitutive relationships for fluid-saturated porous rock relating strain tensor and fluid velocity to the stress field in solid matrix and to the pressure of the fluid. Substituting constitutive relationship into dynamic equations of motion I obtain a wave equation for two compressional waves and for shear wave. In the end I discuss physical meaning of Biot parameters.

2.2 Dynamic poroelastic equations

In this section I reproduce the dynamic equations of motion for a two-phased system consisting of a porous skeletal elastic frame filled with a compressible fluid. Newton's law reads:

$$\rho_s(1-\phi)\ddot{u}_i + \rho_f\phi\ddot{U}_i = f_i \tag{2.1}$$

where u_i is displacement of the solid frame, U_i is displacement of the fluid, ρ_s is density of the solid, ρ_f is density of the fluid, ϕ is porosity and the "force" vector f_i is given by:

$$f_i = \partial_j\sigma_{ij} \tag{2.2}$$

where σ_{ij} is stress tensor.

Rearranging equation (2.1) in terms of displacement of solid u_i and relative displacement of fluid with respect to solid $U_i - u_i$, yields:

$$[\rho_s(1-\phi)\ddot{u}_i + \rho_f\phi\ddot{u}_i] + [\rho_f\phi(\ddot{U}_i - \ddot{u}_i)] = \partial_j\sigma_{ij} \tag{2.3}$$

or, identically:

$$\rho\ddot{u}_i + \rho_f\ddot{\nu}_i = \partial_j\sigma_{ij} \tag{2.4}$$

where $\rho = \rho_s(1-\phi) + \rho_s\phi$ is mean density of the fluid-saturated porous rock and $\dot{\nu}_i = \phi(\dot{U}_i - \dot{u}_i)$ is filtration velocity of the fluid in the moving solid.

Dynamic equation for viscous pore-fluid obeying Darcy's law reads [Stoll 1989]:

$$\rho_f\ddot{U}_i = -\partial_i P - \frac{\eta\phi}{\kappa}(\dot{U}_i - \dot{u}_i) \tag{2.5}$$

where P is pore-fluid pressure, η is fluid viscosity and κ is specific permeability of porous rock.

Rearranging equation (2.5) in a way similar to equation (2.3) yields:

$$\rho_f\ddot{u}_i + \rho_f(\ddot{U}_i - \ddot{u}_i) = -\partial_i P - \frac{\eta\phi}{\kappa}(\dot{U}_i - \dot{u}_i)$$

or, finally:

$$\rho_f\ddot{u}_i + \frac{\rho_f}{\phi}\dot{\nu}_i = -\partial_i P - \frac{\eta}{\kappa}\dot{\nu}_i \tag{2.6}$$

More accurate consideration of fluid movement in permeable porous rock results in an additional parameter c in the second term on the LHS of equation (2.6). This parameter c, known as the 'tortuosity' [Stoll 1989], accounts for the 'sinuous' character of fluid motion at the micro-scale. Defining effective fluid mass-density $m = c\frac{\rho_f}{\phi}$, I obtain a modified version of equation (2.6) for fluid:

$$\rho_f\ddot{u}_i + m\ddot{\nu}_i = -\partial_i P - \frac{\eta}{\kappa}\dot{\nu}_i \tag{2.7}$$

Equations (2.4) and (2.7) are coupled dynamic equations of motion for fluid-saturated poroelastic medium.

2.3 Constitutive relationships for fluid-saturated porous rock

It was suggested by Maurice Biot [1956] that for purely elastic porous solid, the elastic energy density W is a quadratic function of first two invariants $I_1 = e_{ii} = e$ and $I_2 = (e_{ii})^2 - e_{ij}e_{ji}$ of strain tensor e_{ij} and increment ξ of fluid content:

$$W = \frac{H}{2}e^2 - 2\mu I_2 - Ce\xi + \frac{M}{2}\xi^2 \tag{2.8}$$

In equation (2.8) μ is the shear modulus and H, C, M are a set of parameters introduced by Biot (1956). Fluid increment ξ is related to filtration velocity by the following relationship:

$$\xi = -\phi\partial_i(U_i - u_i) = -\partial_i\nu_i \tag{2.9}$$

Differentiation of W over strain tensor and increment of fluid content yields the constitutive relationships for fluid-saturated porous solid:

$$dW = \frac{\partial W}{\partial e_{ij}}de_{ij} + \frac{\partial W}{\partial \xi}d\xi = \sigma_{ij}de_{ij} + Pd\xi \tag{2.10}$$

where stress tensor

$$\sigma_{ij} = [(H - 2\mu)e - C\xi]\delta_{ij} + \mu(\partial_i u_j + \partial_j u_i) \tag{2.11}$$

and pore-fluid pressure

$$P = M\xi - Ce \tag{2.12}$$

are functions of the solid frame displacement u_i and the increment ξ of fluid content.

2.4 Wave equations for compressional waves

By taking the divergence of the equations of motion (2.4) and (2.7) I obtain:

$$\partial_{tt}^2(\rho\partial_i u_i + \rho_f\partial_i\nu_i) = \partial_i\partial_j\sigma_{ij} \tag{2.13}$$

$$\partial_{tt}^2(\rho_f\partial_i u_i + m\partial_i\nu_i) = -\partial_{ii}^2 P - \frac{\eta}{\kappa}\partial_t\partial_i\nu_i \tag{2.14}$$

The substitution of stress tensor σ_{ij} and pore-fluid pressure P defined by constitutive relationships (2.11) and (2.12) yields a coupled system of wave equations for compressional waves where $e = e_{ii} = \partial_i u_i$ and ξ was defined by equation (2.9):

$$\partial_{tt}^2(\rho e - \rho_f \xi) = \Delta(He - C\xi) \tag{2.15}$$

$$\partial_{tt}^2(\rho_f e - m\xi) = -\Delta(M\xi - Ce) + \frac{\eta}{\kappa}\partial_t \xi \tag{2.16}$$

Note that these two equations couple the displacement of solid frame and the relative displacement of viscous fluid which are not independent. The coupled system of equations (2.15) and (2.16) indicates that there are two separate (compressional) modes propagating in a poroelastic medium.

2.5 Wave equation for shear wave

To derive the wave equation for shear waves, I introduce rotational components $\vec{\Omega}$ and $\vec{\Theta}$ of displacement of solid u_i and of relative displacement $U_i - u_i$ of fluid:

$$\vec{\Omega} = \text{curl}(\vec{u}) \qquad \vec{\Theta} = -\phi\text{curl}(\vec{U} - \vec{u}) = -\text{curl}(\vec{\nu}) \tag{2.17}$$

The rotational component of equation (2.7) reads:

$$\partial_{tt}^2(\rho_f \vec{\Omega} - m\vec{\Theta}) = -\underbrace{\text{curl grad}}_{=0} P - \frac{\eta}{\kappa}\text{curl}\dot{\vec{\nu}} \tag{2.18}$$

Rotational component of LHS of (2.4) is given by:

$$\partial_{tt}^2(\rho\vec{\Omega} - \rho_f\vec{\Theta}) \tag{2.19}$$

To find the rotational part of the RHS of equation (2.4) I apply to it the curl operator in the form:

$$[\text{curl}(\vec{A})]_k = \epsilon_{kli}\partial_l A_i \tag{2.20}$$

where $\vec{A}$ is an arbitrary vector and ϵ_{ikl} is Levi-Civita anti-symetric tensor. This and equation (2.11) yield:

$$\begin{aligned} & \epsilon_{kli}\partial_l\partial_j\sigma_{ij} \\ = \;& \epsilon_{kli}\partial_l\partial_j[(H-2\mu)e - C\xi]\delta_{ij} + \mu\epsilon_{kli}\partial_l\partial_j(\partial_i u_j + \partial_j u_i) \\ = \;& \epsilon_{kli}\partial_l\partial_i[(H-2\mu)e - C\xi] + \mu\epsilon_{kli}\partial_l\partial_i(\partial_j u_j) + \mu\partial_{jj}^2\underbrace{(\epsilon_{kli}\partial_l u_i)}_{\Omega_k} \end{aligned} \tag{2.21}$$

The first two terms on the RHS of equation (2.21) vanish due to the antisymetry of Levi-Civita tensor.

Equating expressions (2.19) and (2.21) results, with (2.18), in the equations for the shear wave.

$$\partial_{tt}^2(\rho\vec{\Omega} - \rho_f\vec{\Theta}) = \mu\Delta\vec{\Omega} \tag{2.22}$$

$$\partial_{tt}^2(\rho_f\vec{\Omega} - m\vec{\Theta}) = \frac{\eta}{\kappa}\partial_t\vec{\Theta} \tag{2.23}$$

Wave equations (2.22) and (2.23) describe the propagation of a shear wave in fluid-saturated poroelastic rock. While in equations (2.15-2.16) a laplacian was operating before both variables e and ξ in both equations, here it operates in front of only one variable and therefore yields only one mode of propagation (see equation (3.29)).

2.6 Physical meaning of Biot parameters

There are several different ways to relate Biot's phenomenological parameters H, C and M to physical parameters that can be measured in laboratory experiments (for example, see Bourbie et al. 1986). I will use in my thesis the representation introduced by Stoll [1989]. In this representation, Biot's parameters H, C and M are expressed through the bulk modulus K_r of individual sediment grains, the bulk modulus K_f of pore-fluid and the bulk modulus K_b of porous frame as measured for the case of constant pore-fluid pressure (referred to as 'drained' bulk modulus):

$$H = \frac{(K_r - K_b)^2}{D - K_b} + K_b + 4\mu/3 \tag{2.24}$$

$$C = \frac{K_r(K_r - K_b)}{D - K_b} \tag{2.25}$$

$$M = \frac{K_r^2}{D - K_b} \tag{2.26}$$

where

$$D = K_r(1 + \phi(K_r/K_f - 1)) \tag{2.27}$$

The Gassmann velocities (in the zero-frequency limit) are then given by:

$$\rho V_P^2 = H$$

and

$$\rho V_S^2 = \mu \tag{2.28}$$

Following Stoll [1977, 1989], I will assume the bulk and shear moduli of the frame K_b and μ to be complex constants. The notion of constant complex moduli for crustal rocks has been suggested by a number of authors [Aki and Richards 1980] to take into account visco-elastic behaviour of the skeletal frame of porous solid.

2.7 Summary

The main result of this chapter is given by a system of wave equations (2.15) and (2.16) for compressional wave-field. This coupled system of wave equations clearly indicates that there are two different modes of compressional wave-field propagating in fluid-saturated poroelastic medium. The wave equation for shear waves (2.22)-(2.23) also shows some coupling between solid frame motion in shear wave and pore fluid. Another important result is given by the set of equations (2.24)-(2.27) identifying phenomenological parameters of Biot's theory with physical parameters conventionally measured in laboratory experiments.

Chapter 3

DISPERSION EQUATIONS

3.1 Introduction

In this chapter I derive dispersion equations for compressional and shear harmonic plane waves. I show that there are two kinds of compressional waves propagating in poroelastic medium. One wave is a conventional P-wave. In this wave pore-fluid moves more or less in phase with elastic frame. The compressional wave of second kind predicted by Maurice Biot [Biot 1956] corresponds to the situation where pore-fluid moves out of phase with elastic frame. This results in significant attenuation of this wave caused by relative viscous flow of pore-fluid with respect to solid frame.

In this chapter I define the displacement in solid frame for all types of plane waves as given by:

$$\vec{u} : u_i = a_i \exp(-i\omega q(x + pz)) \exp(i\omega t) = a_i exp(E) \tag{3.1}$$

where q is the horizontal slowness of the wave and p is ratio of vertical over horizontal slowness. I define this ratio as p for the P-wave, b for the Biot wave, s for the S_V wave and ς for the $S_H$wave. Where the solid frame is elastically isotropic and the specific permeability is directionally independent, the pore-fluid displacement is linearly related to the solid frame displacement:

$$\vec{U} = \hat{U}\vec{u} = \hat{U}\vec{a}E \tag{3.2}$$

where $\hat{U}$ is a linear operator introducing a phaseshift between solid frame and fluid displacement. I consider only isotropic poroelastic medium. In this case, the pore-fluid displacement is collinear to the displacement of solid frame [Biot 1956].

3.2 Dispersion equations for P-wave and Biot slow wave

Substitution of plane wave displacement (3.1) yields the expressions for dilatation e and fluid increment ξ in plane waves:

$$e = \mathrm{div}\vec{u} = (a_x\partial_x E + a_y\partial_y E + a_z\partial_z E)\exp(E) \tag{3.3}$$

$$e = (a_x + a_z p)(-i\omega q)\exp(E) \tag{3.4}$$

$$\xi = \phi\mathrm{div}(\vec{u} - \vec{U}) = \phi\mathrm{div}[(1-\hat{U})\vec{u}] = \mathrm{div}(R\vec{u}) = Re \tag{3.5}$$

with

$$R = \phi(1-\hat{U}) \tag{3.6}$$

Substituting (3.1) and (3.2) in the right-hand side of wave equation (2.15) gives

$$\begin{aligned} \nabla^2(He - C\xi) &= \nabla^2[\{H - C\phi(1-\hat{U})\}e] \\ &= [H - CR]\nabla^2 e \\ &= [H - CR](i\omega q)^2(1+p^2)e \end{aligned} \tag{3.7}$$

which I write as

$$\nabla^2(He - C\xi) = [H - CR](i\omega)^2 Xe \tag{3.8}$$

with

$$X = q^2(1+p^2) \tag{3.9}$$

square of the slowness.

The left-hand side of wave equation (2.15) takes the form:

$$\begin{aligned} \partial_{tt}^2(\rho e - \rho_f\xi) &= [\rho - \rho_f R]\partial_{tt}^2 e \\ &= [\rho - \rho_f R](i\omega)^2 e \end{aligned} \tag{3.10}$$

The equality of these two terms for RHS and LHS yields the first of the dispersion equations for the P-wave sector:

$$[H - CR]X = [\rho - \rho_f R] \tag{3.11}$$

or

$$(HX - \rho) + (-CX + \rho_f)R = 0 \tag{3.12}$$

Similarly, substituting plane wave components e and ξ given by (3.1) and (3.2) into the second wave equation (2.16), one obtains the second dispersion equation:

$$(-CX + \rho_f) + (MX - m + i\frac{\eta}{\kappa\omega})R = 0 \tag{3.13}$$

The dispersion equations (3.12) and (3.13) for compressional waves can be presented in the matrix form:

$$\begin{pmatrix} -HX+\rho & CX-\rho_f \\ -CX+\rho_f & MX-m+i\eta/\kappa\omega \end{pmatrix} \begin{pmatrix} 1 \\ R \end{pmatrix} = \begin{pmatrix} 0 \\ 0 \end{pmatrix} \tag{3.14}$$

For the right hand-side of equation (3.14) to be null, the matrix on the left-hand side must be singular and hence its determinant is null. This yields a quadratic equation in the square X of slowness and therefore there are two possible values for the slowness of a compressional wave. The slowness value of lower real part corresponds to the usual P-wave with the fluid moving more or less in phase with the frame, while the slowness value of greater real part corresponds to the wave of the second kind predicted by Biot, with the fluid moving more or less in opposition of phase with the frame [Biot 1962, Rasolofosaon 1990]. When the slowness value of lower real part is taken, equation (3.14) can be solved in R; the solution will be called R_P as it corresponds to the P-wave. In the same way, when I take the slowness value of higher real part I obtain a solution in R which I call R_B, corresponding to the Biot wave.

From considerations of numerical stability, an equivalent form of eqation (3.14) is preferred:

$$\begin{pmatrix} H-CR & \rho-\rho_f R \\ C-MR & \rho_f-m(1-i\eta/m\kappa\omega)R \end{pmatrix} \begin{pmatrix} -X \\ 1 \end{pmatrix} = \begin{pmatrix} 0 \\ 0 \end{pmatrix} \tag{3.15}$$

In this case I first solve equation (3.15) for the parameters R and thereafter obtain the respective squares of slownesses X.

In a low-frequency approximation ($\omega \ll \omega_B$), equation (3.15) yields the following expressions for the parameters R_p and R_b and for the corresponding squares of slownesses X_p and X_b.

$$\begin{aligned} R_p &= i\frac{\omega}{\omega_B}\phi\left(1-\frac{\rho}{\rho_f}\frac{C}{H}\right)+o(\omega) \\ X_p &= \frac{\rho}{H}\left[1-i\epsilon\frac{\omega}{\omega_B}\left(1-\frac{\rho}{\rho_f}\frac{C}{H}\right)^2\right]+o(\omega) \end{aligned} \tag{3.16}$$

and

$$\begin{aligned} R_b &= \frac{H}{C}\left[1+i\frac{\omega}{\omega_B}\phi\left(1-\frac{\rho}{\rho_f}\frac{C}{H}\right)\left(\frac{MH-C^2}{CH}\right)\right]+o(\omega) \\ \frac{\omega}{\omega_B}X_b &= \frac{\rho_f}{C}\left[\frac{\omega}{\omega_B}-i\phi^{-1}\left(\frac{HC}{MH-C^2}\right)\right]+o(\omega) \end{aligned} \tag{3.17}$$

where ω_B is given by (1.1) and $\epsilon = \phi\rho_f/\rho$.

3.3 Dispersion equation for S-wave

For shear waves I substitute expression (3.1) for solid displacement u in a plane wave in equation (2.17) for rotational component $\vec{\Omega}$:

$$\begin{aligned}\vec{\Omega} = \text{curl}\vec{u} &= \begin{pmatrix}\partial_x\\ \partial_y\\ \partial_z\end{pmatrix} \wedge \begin{pmatrix}a_x\\ a_y\\ a_z\end{pmatrix} \exp(E)\\ &= \nabla \wedge \vec{a}\exp(e)\\ &= \begin{pmatrix}(a_z\partial_y - a_y\partial_z)\exp(E)\\ (a_x\partial_z - a_z\partial x)\exp(E)\\ (a_y\partial_x - a_x\partial_y)\exp(E)\end{pmatrix}\\ &= (-i\omega q)\begin{pmatrix}-a_y p\\ a_x p - a_z\\ a_y\end{pmatrix}\exp(E)\end{aligned} \tag{3.18}$$

I can write $\vec{\Omega} = \begin{pmatrix}\omega_x\\ \omega_y\\ \omega_z\end{pmatrix}\exp(E)$, where $\omega_x, \omega_y, \omega_z$ are all coordinate and time independent. Therefore

$$\partial_t\vec{\Omega} = \partial_t\left[\begin{pmatrix}\omega_x\\ \omega_y\\ \omega_z\end{pmatrix}\exp(E)\right] = \begin{pmatrix}\omega_x\\ \omega_y\\ \omega_z\end{pmatrix}[(\partial E)\exp(E)] \tag{3.19}$$

and

$$\partial_t\vec{\Omega} = (i\omega)\vec{\Omega} \tag{3.20}$$

Similarly

$$\nabla^2\vec{\Omega} = (\nabla^2 E)\vec{\Omega} = -(\omega q)^2(1+p^2)\vec{\Omega} \tag{3.21}$$

and

$$\nabla^2\vec{\Omega} = (i\omega)^2 X\vec{\Omega} \tag{3.22}$$

The rotational component $\vec{\Theta}$ of the fluid displacement relative to the solid displacement is given by:

$$\begin{aligned}\vec{\Theta} &= \phi\text{curl}(\vec{u} - \vec{U}) &&= \phi\text{curl}[(1-\hat{U})\vec{u}]\\ &= \text{curl}[\phi(1-\hat{U})\vec{u}] &&= \text{curl}(R\vec{u})\end{aligned} \tag{3.23}$$

and

$$\vec{\Theta} = R\vec{\Omega} \tag{3.24}$$

Substituting (3.14), (3.19) and (3.21) in the rotational components of the wave equations (2.22) and (2.23), I obtain:

$$(i\omega)^2[\rho - \rho_f R]\vec{\Omega} = \mu(i\omega)^2 X\vec{\Omega} \tag{3.25}$$

$$(i\omega)^2[\rho_f - mR]\vec{\Omega} = \frac{\eta}{\kappa}(i\omega)R\vec{\Omega} \tag{3.26}$$

or:

$$\rho - \mu X - \rho_f R = 0 \tag{3.27}$$

$$\rho_f + \left[-m + \frac{i\eta}{\kappa\omega}\right] R = 0 \tag{3.28}$$

For shear waves I can then write the dispersion equation in a matrix form:

$$\begin{pmatrix} -\mu X + \rho & -\rho_f \\ \rho_f & -m + i\eta/\omega\kappa \end{pmatrix} \begin{pmatrix} 1 \\ R \end{pmatrix} = \begin{pmatrix} 0 \\ 0 \end{pmatrix} \tag{3.29}$$

This equation gives us only one solution in X which corresponds to only one mode of shear waves as in the viscoelastic case. However, although the propagation of a shear wave in the bulk of fluid-saturated poroelastic material obeys a viscoelastic behaviour, at an interface the shear wave interacts with both P-wave and *Biot* wave. This is an effect specific to the fluid-saturated poroelastic materials.

3.4 Numerical results for dispersion equations

To illustrate the effect of dispersion on phase velocities and attenuations I use the set of model parameters proposed by Crampin and Taylor [1998]. Table 3.1 lists petrophysical parameters for five different types of unconsolidated sediments.

Table 3.1

	Medium 1	*Medium 2*	*Medium 3*	*Medium 4*	*Medium 5*
K_r (GPa)	36.0	36.0	36.0	36.0	36.0
ρ_r $(g.cm^{-3})$	2.3	2.3	2.6	2.6	2.6
K_f (GPa)	2.0	2.0	2.0	2.0	2.0
ρ_f $(g.cm^{-3})$	1.0	1.0	1.0	1.0	1.0
η (cP)	0.01	0.01	0.01	0.01	0.01
K_b (GPa)	0.012	0.012	0.044	0.8	1.38
μ (GPa)	0.022	0.022	0.26	0.4	0.83
ϕ	0.76	0.76	0.4	0.4	0.47
c	1.25	1.25	1.25	1.25	1.25
k (cm^2)	$0.26\ 10^{-10}$	$0.1\ 10^{-6}$	$0.1\ 10^{-5}$	$0.1\ 10^{-5}$	$0.1\ 10^{-6}$
δ	0.5	0.5	0.005	0.005	0.47

In this table K_r is the individual grain bulk modulus, ρ_r is the grain density, K_f is the fluid bulk modulus, ρ_f is the fluid density, η is the fluid viscosity, K_b is the bulk modulus of the skeleton frame, μ is the shear modulus of the frame, ϕ is the porosity, c is the tortuosity, k is the permeability, δ is the log decrement and a is the pore size.

Complex values of K_b and μ are introduced through the log decrement δ in order to account for the attenuation in the solid frame with: $\bar{K}_b = K_b(1 + i\delta)$ and $\bar{\mu} = \mu(1 + i\delta)$. The frequency dependence of the attenuation of seismic waves is a controversial issue in the literature [Aki and Richards 1980]. Although a constant attenuation factor is often observed in experiments with dry solids, an attenuation factor strictly constant at all frequencies violates the causality principle and is not compatible with Futterman's relationships between dispersion and attenuation [O'Donnell et al. 1978]. Following Stoll [1989] we consider a constant δ to be reasonable to model most sediments in a finite frequency range; it should be noted that although δ is constant, our model produces frequency dependent attenuation factors.

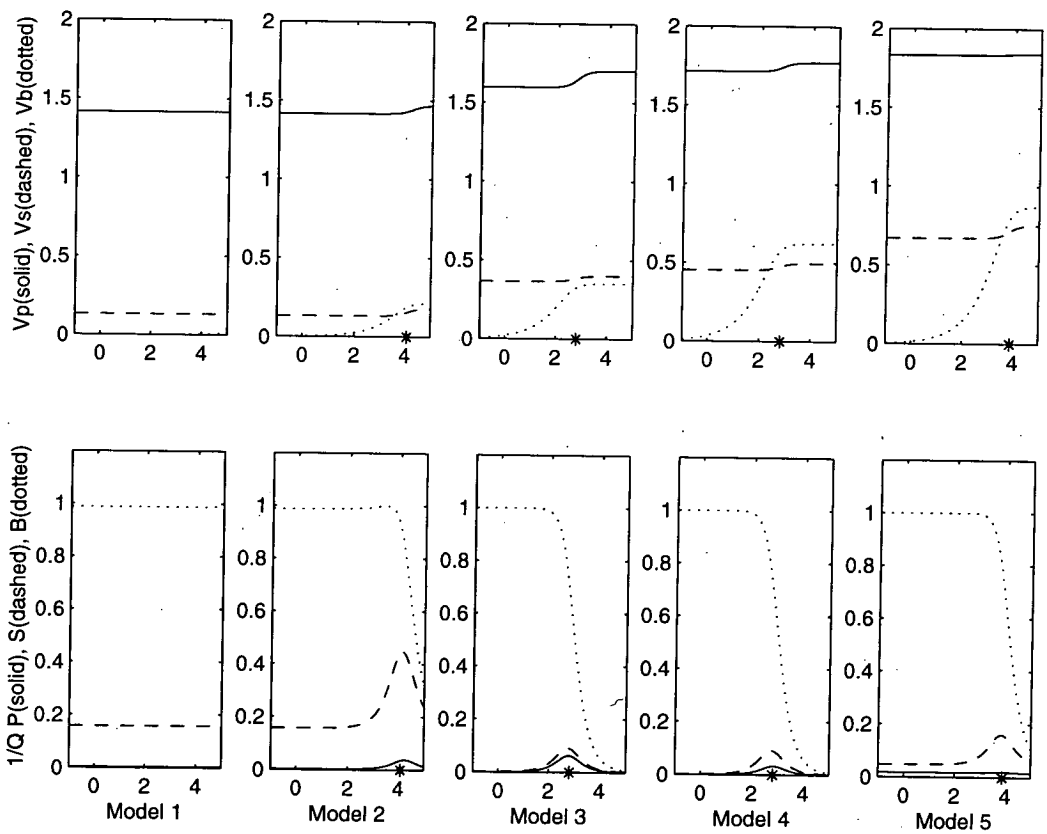

Figure 3.1: Phase velocity V and attenuation Q^{-1} as a function of log frequency; from $0.1Hz$ to $100KHz$ for five different models given in table 3.1. Solid lines correspond to P-wave, dashed lines to S-wave and dotted lines to Biot wave. Asterisk indicates Biot frequency

The first and second media are given with the parameters appropriate for fine mud, the third and fourth - for fine sand and the fifth medium - for coarse sand.

The behaviour of P-wave and S-wave are similar. The velocities increase with frequency as approaching the characteristic Biot frequency at which the attenuation factors show a peak.

3.5 Summary

The main results of this chapter are the dispersion equations for compressional and shear waves given by the matrix equations (3.14) and (3.29) respectively. It follows from the dispersion equation (3.14) that for a given frequency we have two solutions for the slowness of compressional wave. For relatively low frequency the lower value of slowness corresponds to the usual P-wave while the greater value of slowness corresponds to the compressional wave of second kind predicted by Maurice Biot in 1956. In this way fluid moves out of phase with the elastic frame. Numerical results shown in Figure 3.1 indicate that the effects caused by Biot wave can be observed only at relatively high frequencies for conventional sedimentary rocks.

Chapter 4

DECOMPOSITION OF WAVE FIELD INTO UPGOING AND DOWNGOING COMPONENTS

4.1 Introduction

In this chapter I show how to decompose seismic wave field in poroelastic medium into upgoing and downgoing components for different types of waves. I follow closely the approach developed by David Taylor [1977].

I define the displacement in a plane harmonic wave as:

$$u_i(t) = a_i(\omega) \exp(i\omega t) \exp[-i\omega \vec{k} \cdot \vec{r}] \tag{4.1}$$

where for P-wave the slowness vector is $\vec{k} = q(1\ 0\ p)^T$ for a downgoing component, and $\vec{k} = q(1\ 0\ -p)^T$ for an upgoing component of wave field and $a_i(\omega)$ is the polarisation vector. In equation (4.1) q is the horizontal slowness and p is the ratio of vertical over horizontal slowness. Such an upgoing/downgoing decomposition is valid in all cases, except when the wave propagates horizontally (in which case the angle of incidence is $\pi/2$).

The propagation of seismic wave through a plane interface is determined by boundary conditions for displacements, tractions, fluid filtration velocities and pore fluid pressure on both sides of the interface, with explicit knowledge of which part of the wave motion is related to which particular wave-field component.

Therefore, it is necessary to obtain a decomposition of seismic wave-field into upgoing and downgoing wave components with explicitly known polarisation vectors and associated stress in fluid-saturated porous medium. In the case of fluid-saturated porous medium wave-field

must include additional components related to the fluid filtration velocity and pressure. In this chapter I decompose the propagating wave in the porous medium in four upgoing waves and four downgoing waves: compressional wave (P), Biot wave (B), S_V wave (S) and S_H wave (Z). The polarisations of these waves are deduced from the constitutive equations (2.11) and (2.12).

4.2 Compressional wave components

For a downgoing P-wave, the displacement $\vec{u}$ is collinear to the slowness $\vec{k}$ and I can write:

$$\vec{u} = \frac{\exp(E)}{\sqrt{1+p^2}} \begin{pmatrix} 1 \\ 0 \\ p \end{pmatrix} \tag{4.2}$$

where $\vec{u}$ is normalised and p is the cotangent of the angle of incidence. Dilatation e is given by:

$$e = div(\vec{u}) = \partial_x u_x + \partial_y u_y + \partial_z u_z = -i\omega q\sqrt{1+p^2}\exp(E) \tag{4.3}$$

To obtain the traction components, i.e. the components of stress tensor at the surface of horizontal interface, I substitute equation (4.1) into equation (2.11):

$$\begin{aligned} \sigma_{xz} &= \mu(\partial_z u_x + \partial_x u_z) \\ &= \frac{-i\omega q}{\sqrt{1+p^2}}\mu(p+p)\exp(E) = -i\omega q\frac{2p\mu}{\sqrt{1+p^2}}\exp(E) \end{aligned} \tag{4.4}$$

$$\sigma_{yz} = 0 \quad as \quad \partial_y u_z = 0 = u_y \tag{4.5}$$

$$\begin{aligned} \sigma_{zz} &= [He - 2\mu(\partial_x u_x + \partial_y u_y) - C\xi] \\ &= [(H - CR_P)e - 2\mu\partial_x u_x] \\ &= [(H - CR_P)(1+p^2) - 2\mu]\exp(E)(-\tfrac{i\omega q}{\sqrt{1+p^2}}) \end{aligned} \tag{4.6}$$

To calculate R_P, one must solve the dispersion equation (3.14) quadratic in X, the square of the slowness. Choosing X corresponding to the slowness with the lowest real part, I can find the eigenvector $(1, R)^T = (1, R_P)^T$ corresponding to P-wave.

Summing up equations (4.4), (4.5) and (4.6), I present the traction components in the form of a vector $\vec{l}$:

$$\vec{l} = \begin{pmatrix} \sigma_{xz} \\ \sigma_{yz} \\ \sigma_{zz} \end{pmatrix} = -\frac{i\omega q}{\sqrt{1+p^2}}\exp(E) \begin{pmatrix} 2p\mu \\ 0 \\ (H - CR_P)(1+p^2) - 2\mu \end{pmatrix} \tag{4.7}$$

z-component of filtration velocity is obtained by substituting (4.1) into equation (3.5):

$$\dot{\xi}_z = [\phi(1-\hat{U})\dot{\vec{u}}]_z = (R_P\dot{\vec{u}})_z = i\omega R_P u_z \tag{4.8}$$

Pore-fluid pressure is obtained by substituting equation (4.1) into equation (2.12):

$$P = M\xi - Ce = (MR_P - C)e = (-i\omega q)(MR_P - C)\exp(E)\sqrt{1+p^2} \tag{4.9}$$

The upgoing wave-components are derived replacing $\vec{k} = q(1\ 0\ p)^T$ by $\vec{k} = q(1\ 0\ -p)^T$ This yields the displacement vector

$$\vec{u} = \frac{\exp(-i\omega q(x-pz)+i\omega t)}{\sqrt{1+p^2}} \begin{pmatrix} -1 \\ 0 \\ p \end{pmatrix} \tag{4.10}$$

For the *B*iot (slow) wave, the derivations are exactly the same as for the *P*-wave, except that the cotangent of the angle between wave vector and vertical axis z is different and defined as b, and that the highest value of the slowness is taken when solving dispersion equation (3.14), leading to the eigenvector R_B.

4.3 Shear wave components

In shear wave the displacement vector $\vec{u}$ is perpendicular to $\vec{k}$ and the dilatation e vanishes:

$$e = div\vec{u} = -i\omega\vec{k}\cdot\vec{u} = 0 \tag{4.11}$$

The pore-fluid pressure vanishes too, as can be seen by substituting equation (4.3) into equation (3.12):

$$P = M\xi - Ce = (MR_S - C)e = 0 \tag{4.12}$$

where R_S is the second component of the eigenvector in the dispersion equation (3.26) (solved for a given frequency). As in a conventional isotropic case, the shear wave sector is represented by two waves: an S_V wave with displacement in the (x,z) plane and an S_H-wave for which the displacement is perpendicular to that plane.

For the downgoing vertical shear wave S_V I write the displacement vector:

$$\vec{u} = \frac{\exp(E)}{\sqrt{1+s^2}} \begin{pmatrix} -s \\ 0 \\ 1 \end{pmatrix} \quad \vec{k} = \begin{pmatrix} 1 \\ 0 \\ s \end{pmatrix} \tag{4.13}$$

where s is the cotangent of the angle of incidence. The components of traction associated with the wave are:

$$\sigma_{xz} = \mu(\partial_x u_z + \partial_z u_x) = -i\omega q \frac{\mu(1-s^2)}{\sqrt{1+s^2}} \exp(E) \tag{4.14}$$

$$\sigma_{yz} = 0$$

and

$$\sigma_{zz} = [(H - CR)e - 2\mu(\partial_x u_x + \partial_y u_y)]$$

which reduces to

$$\sigma_{zz} = -2\mu\partial_x u_x = i\omega q \frac{2\mu s}{\sqrt{1+s^2}} \exp(E) \tag{4.15}$$

These traction components can be presented in the form of a vector $\vec{l}$:

$$\vec{l} = \begin{pmatrix} \sigma_{xz} \\ \sigma_{yz} \\ \sigma_{zz} \end{pmatrix} = -\frac{i\omega q}{\sqrt{1+s^2}} \exp(E) \begin{pmatrix} \mu(1-s^2) \\ 0 \\ -2\mu s \end{pmatrix} \tag{4.16}$$

Filtration velocity $\dot{\xi}_z$ is obtained by substituting (4.1) into (3.5)

$$\dot{\xi}_z = [\phi(1-\hat{U})\dot{\vec{u}}]_z = (R_s\dot{\vec{u}})_z = i\omega R_s u_z \tag{4.17}$$

where R_S is solution in R of the dispersion equation (3.26) for a given frequency.

For upgoing shear waves the derivation is similar with the slowness vector $\vec{k} = q(1\ 0\ -s)^T$, and the polarisation vector is

$$\vec{u} = \frac{\exp(-i\omega q(x - sz) + i\omega t)}{\sqrt{1+s^2}} \begin{pmatrix} s \\ 0 \\ 1 \end{pmatrix} \tag{4.18}$$

The calculations are exactly the same as for the downgoing wave, the only difference is due to the opposite sign in the first component of displacement vector $\vec{u}$ and in the last component of traction $\vec{l}$ compared with the results for downgoing S_V waves.

For downgoing horizontal shear wave S_H, I take:

$$\vec{u} = \begin{pmatrix} 0 \\ 1 \\ 0 \end{pmatrix} \exp(E); \quad \vec{k} = \begin{pmatrix} 1 \\ 0 \\ \varsigma \end{pmatrix} \tag{4.19}$$

Since $u_x = U_z = 0$, only one component of traction does not vanish:

$$\sigma_{yz} = \mu\partial_z u_y = (i\omega q)\mu\varsigma \exp(E) \tag{4.20}$$

and the traction vector is:

$$\vec{l} = \begin{pmatrix} 0 \\ \sigma_{yz} \\ 0 \end{pmatrix} = \exp(E) \begin{pmatrix} 0 \\ (i\omega q)\mu\varsigma \\ 0 \end{pmatrix} \tag{4.21}$$

The filtration velocity and fluid pressure associated with S_H-wave vanish.

Similarly, for upgoing horizontal shear wave S_H:

$$\vec{u} = \exp(E) \begin{pmatrix} 0 \\ 1 \\ 0 \end{pmatrix}; \quad \vec{k} = \begin{pmatrix} 1 \\ 0 \\ -\varsigma \end{pmatrix} \tag{4.22}$$

and

$$\vec{l} = \begin{pmatrix} 0 \\ \sigma_{yz} \\ 0 \end{pmatrix} = \begin{pmatrix} 0 \\ \mu\partial_z u_y \\ 0 \end{pmatrix} = \exp(E) \begin{pmatrix} 0 \\ -(i\omega q)\mu\varsigma \\ 0 \end{pmatrix} \tag{4.23}$$

4.4 Final results

In tables 4.1-4.4 I provide a complete list of downgoing ($\downarrow$) and upgoing ($\uparrow$) wave-field components for P-, Biot(B)-, $S_V(S)$- and $S_H(Z)$-waves.

Table 4.1

	$P\downarrow$	$P\uparrow$
Displacement	$\frac{1}{\sqrt{1+p^2}} \begin{pmatrix} 1 \\ 0 \\ p \end{pmatrix}$	$\frac{1}{\sqrt{1+p^2}} \begin{pmatrix} -1 \\ 0 \\ p \end{pmatrix}$
$\frac{Tract.\sqrt{1+p^2}}{-i\omega q}$	$\begin{pmatrix} 2\mu p \\ 0 \\ (1+p^2)(H - R_P C) - 2\mu \end{pmatrix}$	$\begin{pmatrix} 2\mu p \\ 0 \\ -(1+p^2)(H - R_P C) + 2\mu \end{pmatrix}$
Filtrat. veloc.	$i\omega R_P p/\sqrt{1+p^2}$	$i\omega R_P p/\sqrt{1+p^2}$
Fluid pressure	$(-i\omega q)(MR_P - C)\sqrt{1+p^2}$	$-(-i\omega q)(MR_P - C)\sqrt{1+p^2}$

Table 4.2

	$B\downarrow$	$B\uparrow$
Displacement	$\frac{1}{\sqrt{1+b^2}}\begin{pmatrix}1\\0\\b\end{pmatrix}$	$\frac{1}{\sqrt{1+b^2}}\begin{pmatrix}-1\\0\\b\end{pmatrix}$
$\frac{Tract.\sqrt{1+b^2}}{-i\omega q}$	$\begin{pmatrix}2\mu b\\0\\(1+b^2)(H-R_BC)-2\mu\end{pmatrix}$	$\begin{pmatrix}2\mu b\\0\\-(1+b^2)(H-R_BC)+2\mu\end{pmatrix}$
Filtrat. veloc.	$i\omega R_B b/\sqrt{1+b^2}$	$i\omega R_B b/\sqrt{1+b^2}$
Fluid pressure	$(-i\omega q)(MR_B-C)\sqrt{1+b^2}$	$-(-i\omega q)(MR_B-C)\sqrt{1+b^2}$

Table 4.3

	$S\downarrow$	$S\uparrow$
Displacement	$\frac{1}{\sqrt{1+s^2}}\begin{pmatrix}-s\\0\\1\end{pmatrix}$	$\frac{1}{\sqrt{1+s^2}}\begin{pmatrix}s\\0\\1\end{pmatrix}$
$\frac{Tract.\sqrt{1+s^2}}{-i\omega q}$	$\begin{pmatrix}\mu(1-s^2)\\0\\2\mu s\end{pmatrix}$	$\begin{pmatrix}\mu(1-s^2)\\0\\-2\mu s\end{pmatrix}$
Filtrat. veloc.	$i\omega R_S/\sqrt{1+s^2}$	$i\omega R_S/\sqrt{1+s^2}$
Fluid pressure	0	0

Table 4.4

	$Z\downarrow$	$Z\uparrow$
Displacement	$\begin{pmatrix}0\\1\\0\end{pmatrix}$	$\begin{pmatrix}0\\1\\0\end{pmatrix}$
$Tract./(-i\omega q)$	$\begin{pmatrix}0\\\mu\varsigma\\0\end{pmatrix}$	$\begin{pmatrix}0\\-\mu\varsigma\\0\end{pmatrix}$
Filtrat. veloc.	0	0
Fluid pressure	0	0

4.5 Wave energy flux

The averaged (over wave period) flux of energy across a unit area of surface with normal $\vec{n}$ is given as a work done by traction component and pressure on that element of surface (solid frame+pore fluid):

$$E = \int_t^{t+2\pi/\omega} Re(\sigma_{ij} \cdot \dot{u}_i^* + P_f \dot{U}_j^*) n_j dt \tag{4.24}$$

$$E = -\frac{1}{2} Re(\sigma_{ij} \cdot u_i^* + P_f U_j^*) n_j \tag{4.25}$$

where u is displacement of solid, σ is stress tensor, P_f is pore-fluid pressure and U_i is displacement of fluid [Stoll 1977]. Using results from tables (4.1 - 4.4) I obtain expressions for energy flux in the direction of wave propagation for P-, Biot- and S-waves as the real parts of following expressions:

$$\begin{aligned} E_P &= \omega^2 s_p (H - 2Re(R_P)C + M R_P R_P^*) \\ E_B &= \omega^2 s_b (H - 2Re(R_B)C + M R_B R_B^*) \\ E_S &= \omega^2 s_s \mu \end{aligned} \tag{4.26}$$

where s_p, s_b, s_s are the respective slownesses of P-, Biot and S-waves.

4.6 Summary

The main result of this chapter is given by tables 4.1-4.4 for upgoing and downgoing wave-field components of all types of waves: P-waves, Biot waves, SV-waves and SH waves. These tables provide explicit values for displacement and traction components in elastic frame as well as pore-fluid pressure and fluid filtration velocity associated with each type of propagating waves. I use these results together with boundary conditions to derive a general matrix equation for reflection and transmission coefficients at the interface between two fluid-saturated poroelastic media.

Chapter 5

REFLECTIONS AND TRANSMISSIONS IN POROELASTICITY

5.1 Introduction

In the dynamic theory of elasticity the displacement vector u_i and the stress traction components σ_{xz}, σ_{yz} and σ_{zz} are continuous accros the horizontal interface between two elastic media. These six elastic conditions are obviously not enough to describe the reflection or trasmission of waves in fluid-saturated poroelastic medium. Then, additional conditions must be introduced to relate pore-fluid velocity and pressure on each side of the interface. Deresiewicz and Skalak [1963] extended Neumann's boundary conditions [Dautray and Lions 1984] for wave propagation in elastic solids to fluid-saturated porous solids. They have shown that the normal component of filtration velocity is continuous accross the interface between two fluid-saturated poroelastic solids, while in a general case of partially sealed interface pore-fluid pressure experiences a discontinuity proportional to the vertical component of filtration velocity (fluid flow accross the interface) with a coefficient of proportionality κ_s characterising the hydraulic transmissivity of the partially sealed interface.

Later on, Bourbie et al. [1986] have given a proof of these boundary conditions on the basis of Hamilton's principle. For some situations the boundary conditions suggested by Deresiewicz and Skalak have been verified experimentally [Rasolofosaon 1988, Gurevich 1996]. However, Gurevich and Schoenberg [1999] argued that these Deresiewicz and Skalak's interface conditions for pore-fluid pressure discontinuity across partially sealed interface is not fully consistent with the validity of Biot's equations. They stated that only open-pore interface conditions (perfectly permeable interface) are consistent with the validity of Biot's theory equations. They consider that the partially sealed interface should be treated as a fine layer of finite permeability. In this

case one can expect discontinuity not only in pore-fluid pressure but also in the displacement and traction components across the interface.

Notwithstanding Gurevich and Schoenberg [1999] criticism, I use in my thesis the boundary conditions suggested by Deresiewicz and Skalak [1963] for two main reasons. First, these conditions are found to be very useful in experiments. Second, in sedimentary rocks the change in hydraulic permeability is several (up to ten) orders of magnitude at the lengthscale of a few mms. It is easy to imagine a very thin layer (film) with very low permeability, effectively creating an essential drop in fluid pressure for a given pore-fluid flow while not strongly affecting displacement and stress components.

The eight boundary conditions of Deresiewicz and Skalak [1963] are sufficient to couple the upgoing and downgoing components of all types of waves at the horizontal interface. In this chapter I show how to derive a set of matrix equations for reflection and transmission coefficients for all types of waves (P-wave, Biot wave, S_V wave and S_H wave) across a horizontal interface with Deresiewicz and Skalak [1963] conditions. Because S_H wave is uncoupled from other waves (in isotropic medium), I review this case separately and then I show how to generalise it to the case of P-wave, Biot wave and S_V wave which are coupled at the horizontal interface.

5.2 Boundary conditions

According to Deresiewiecz and Skalak [1963], for perfectly permeable interface the boundary conditions at the interface between fluid-saturated porous media are given by:

$$u_i^{(1)} = u_i^{(2)}; \qquad \sigma_{iz}^{(1)} = \sigma_{iz}^{(2)}; \qquad \dot{\xi}_z^{(1)} = \dot{\xi}_z^{(2)}; \qquad P_f^{(1)} = P_f^{(2)} \tag{5.1}$$

where index 1 corresponds to the medium above the horizontal interface and index 2 refers to the medium below the interface.

If the fluid cannot cross the interface freely there is a discontinuity of pore-fluid pressure proportional to the filtration velocity by $1/\kappa_s$ and the last boundary condition in (5.1) is corrected to take into account the pore-pressure drop across the interface:

$$P_f^{(1)} = \left(P_f^{(2)} + \frac{\dot{\xi}_z^{(2)}}{\kappa_s} \right) \tag{5.2}$$

or using the third condition in equation (5.1):

$$\left(P_f^{(1)} - \frac{\dot{\xi}_z^{(1)}}{2\kappa_s} \right) = \left(P_f^{(2)} + \frac{\dot{\xi}_z^{(2)}}{2\kappa_s} \right) \tag{5.3}$$

The terms proportional to the fluid filtration velocity component across the interface account for hydraulic transmissivity of the interface described by an additional 'interface permeability' parameter κ_s. This term is important if the interface is partially sealed.

To implement the upgoing/downgoing wave decomposition derived in the previous chapter, I describe the elements on both sides of equations (5.1) and (5.3) as a sum of an downgoing component (written with a grave accent) and an upgoing component (written with an acute accent). For instance, the components of displacement in solid frame can be decomposed into the sum of two components: $u_i = \grave{u}_i + \acute{u}_i$

This yields the following representations of boundary conditions (5.1) and (5.3):

$$\begin{gathered}
\grave{u}_i^{(1)} + \acute{u}_i^{(1)} = \acute{u}_i^{(2)} + \grave{u}_i^{(2)} \\
\grave{\sigma}_{iz}^{(1)} + \acute{\sigma}_{iz}^{(1)} = \acute{\sigma}_{iz}^{(2)} + \grave{\sigma}_{iz}^{(2)} \\
\dot{\grave{\xi}}_z^{(1)} + \dot{\acute{\xi}}_z^{(1)} = \dot{\acute{\xi}}_z^{(2)} + \dot{\grave{\xi}}_z^{(2)} \\
\dot{\grave{P}}_f^{(1)} + \dot{\acute{P}}_f^{(1)} - \tfrac{1}{2\kappa_s}\left(\dot{\grave{\xi}}_z^{(1)} + \dot{\acute{\xi}}_z^{(1)}\right) = \dot{\acute{P}}_f^{(2)} + \dot{\grave{P}}_f^{(2)} + \tfrac{1}{2\kappa_s}\left(\dot{\acute{\xi}}_z^{(2)} + \dot{\grave{\xi}}_z^{(2)}\right)
\end{gathered} \tag{5.4}$$

Before addressing the more complicated problem of Reflection/Transmission/Conversion coefficients of P-wave, Biot wave and S_V-wave coupled at the interface, I consider the relatively more simple case of S_H-wave.

5.3 S_H wave

The only non-vanishing component of displacement associated with propagating horizontal shear-wave is u_y. I write the downgoing component $\grave{u}_y$ and the upgoing component $\acute{u}_y$ in the following form:

$$\begin{aligned}
\grave{u}_y &= \grave{Z}\exp[-i\omega q(x+\varsigma z) + i\omega t] = \grave{Z}\exp(-i\omega q\varsigma z)\exp[i\omega(-qx+t)] \\
\acute{u}_y &= \acute{Z}\exp[-i\omega q(x-\varsigma z) + i\omega t] = \acute{Z}\exp(+i\omega q\varsigma z)\exp[i\omega(-qx+t)]
\end{aligned} \tag{5.5}$$

where $\grave{Z}$ and $\acute{Z}$ are the respective amplitudes of the downgoing and upgoing components, q is the horizontal slowness and ς is the ratio of vertical over horizontal slowness for the downgoing wave. The downgoing wave is taken as reference and then the second equation in (5.5) gives the upgoing wave. The dispersion equation gives the square X of slowness and, therefore, provides two opposite values for vertical slowness (with one value for a downgoing wave and another value for an upgoing wave):

$$q\varsigma = \pm\sqrt{X - q^2} \tag{5.6}$$

where X is found from equation (3.26):

$$\mu X = \rho - \rho_f^2 \frac{1}{m - i\eta/\omega\kappa} \tag{5.7}$$

The value which has to be chosen is the positive square root, such that its real part is positive and its imaginary part is negative. In the case of an original incident shear wave, ς can be chosen as a real parameter equal to the cotangent of the angle of incidence.

Substitution of the expression for displacement components of equation (5.5) into the constitutive equation (2.11), gives upgoing and downgoing components of traction:

$$\begin{aligned} \grave{\sigma}_{yz} &= \mu \frac{\partial \grave{u}_y}{\partial z} = -\mu i\omega\varsigma \grave{u}_y = -\mu\varsigma \grave{Z} i\omega q \exp(-i\omega q\varsigma z) \exp[i\omega(-qx+t)] \\ \acute{\sigma}_{yz} &= \mu \frac{\partial \acute{u}_y}{\partial z} = \mu i\omega\varsigma \acute{u}_y = \mu\varsigma \acute{Z} i\omega q \exp(i\omega q\varsigma z) \exp[i\omega(-qx+t)] \end{aligned} \tag{5.8}$$

The constitutive equation also yields the filtration velocity and fluid pressure vanishing for S_H-wave.

For the horizontal interface with vertical coordinate $z = 0$, boundary relationships (5.4) become:

$$\begin{aligned} \grave{Z}_1 + \acute{Z}_1 &= \acute{Z}_2 + \grave{Z}_2 \\ -\mu_1\varsigma_1 \grave{Z}_1 + \mu_1\varsigma_1 \acute{Z}_1 &= \mu_2\varsigma_2 \acute{Z}_2 - \mu_2\varsigma_2 \grave{Z}_2 \end{aligned} \tag{5.9}$$

Collecting the emergent wave components ($\acute{Z}_1$ and $\grave{Z}_2$) on the left-hand side and the incident wave components ($\grave{Z}_1$ and $\acute{Z}_2$) on the right-hand side of the system of equations (5.9) yields:

$$\begin{aligned} \acute{Z}_1 - \grave{Z}_2 &= -\grave{Z}_1 + \acute{Z}_2 \\ \mu_1\varsigma_1 \acute{Z}_1 + \mu_2\varsigma_2 \grave{Z}_2 &= \mu_1\varsigma_1 \grave{Z}_1 + \mu_2\varsigma_2 \acute{Z}_2 \end{aligned} \tag{5.10}$$

I can write this result in a matrix form:

$$\begin{pmatrix} 1 & -1 \\ \mu_1\varsigma_1 & \mu_2\varsigma_2 \end{pmatrix} \begin{pmatrix} \acute{Z}_1 \\ \grave{Z}_2 \end{pmatrix} = \begin{pmatrix} -1 & 1 \\ \mu_1\varsigma_1 & \mu_2\varsigma_2 \end{pmatrix} \begin{pmatrix} \grave{Z}_1 \\ \acute{Z}_2 \end{pmatrix} \tag{5.11}$$

The reflection coefficient $R_{\grave{Z}\acute{Z}}$ in the upper medium 1, is defined as the ratio of amplitude $\acute{Z}_1$ of the reflected wave in medium 1 over amplitude $\grave{Z}_1$ of the incident wave in medium 1. The transmission coefficient $T_{\grave{Z}\grave{Z}}$ from upper medium 1 to lower medium 2, is the ratio of amplitude $\grave{Z}_2$ of the transmitted wave in the medium 2 over amplitude $\grave{Z}_1$ of a wave incident on the interface from medium 1.

$$R_{\grave{Z}\acute{Z}} = \left.\frac{\acute{Z}_1}{\grave{Z}_1}\right|_{\acute{Z}_2=0} \quad \text{and} \quad T_{\grave{Z}\grave{Z}} = \left.\frac{\grave{Z}_2}{\grave{Z}_1}\right|_{\acute{Z}_2=0} \tag{5.12}$$

It follows from equation (5.11) that these coefficients are given by the solution of the following matrix equation:

$$\begin{pmatrix} 1 & -1 \\ \mu_1\varsigma_1 & \mu_2\varsigma_2 \end{pmatrix} \begin{pmatrix} R_{\grave{Z}\acute{Z}} \\ T_{\acute{Z}\grave{Z}} \end{pmatrix} = \begin{pmatrix} -1 & 1 \\ \mu_1\varsigma_1 & \mu_2\varsigma_2 \end{pmatrix} \begin{pmatrix} 1 \\ 0 \end{pmatrix} \tag{5.13}$$

where I have set the incident field vector $(\grave{Z}_1 \quad \acute{Z}_2)^T$ to $(1 \quad 0)^T$ representing only one incident wave of unit amplitude.

Similarly when $(\grave{Z}_1 \quad \acute{Z}_2)^T$ is set to $(0 \quad 1)^T$, equation (5.11) yields the other two coefficients for the S_H-wave case:

$$\begin{pmatrix} 1 & -1 \\ \mu_1\varsigma_1 & \mu_2\varsigma_2 \end{pmatrix} \begin{pmatrix} T_{\acute{Z}\grave{Z}} \\ R_{\acute{Z}\acute{Z}} \end{pmatrix} = \begin{pmatrix} -1 & 1 \\ \mu_1\varsigma_1 & \mu_2\varsigma_2 \end{pmatrix} \begin{pmatrix} 0 \\ 1 \end{pmatrix} \tag{5.14}$$

I note that the vectors on the right-hand sides of equations (5.13) and (5.14) are the columns of the identity matrix. I can then gather these two equations in one matrix equation:

$$\begin{pmatrix} 1 & -1 \\ \mu_1\varsigma_1 & \mu_2\varsigma_2 \end{pmatrix} R = \begin{pmatrix} -1 & 1 \\ \mu_1\varsigma_1 & \mu_2\varsigma_2 \end{pmatrix} \tag{5.15}$$

where R is the matrix of reflection and transmission coefficients:

$$R = \begin{pmatrix} R_{\grave{Z}\acute{Z}} & T_{\acute{Z}\acute{Z}} \\ T_{\grave{Z}\grave{Z}} & R_{\acute{Z}\grave{Z}} \end{pmatrix} \tag{5.16}$$

Note that columns in the matrices of equation (5.15) are 2-vectors with components continuous across the interface. I will show in next section that similar matrix equation for reflection coefficients in general case of P-,$Biot$ and S-waves exists where the columns in matrices are given by 6-vectors of continuous components of wave-field.

Figure (5.1) shows the behaviour of complex reflection and transmission coefficients for different angles of incidence for the model described in section (3.4) where the upper medium corresponds to medium 3 and the lower medium corresponds to medium 4 in table (3.1). The critical angle θ_0 is equal to 57°. Dashed line corresponds to purely elastic case. Solid line shows the effect of poroelasticity which for S_H waves is identical to some visco-elastic corrections (see dispersion equation (3.29)).

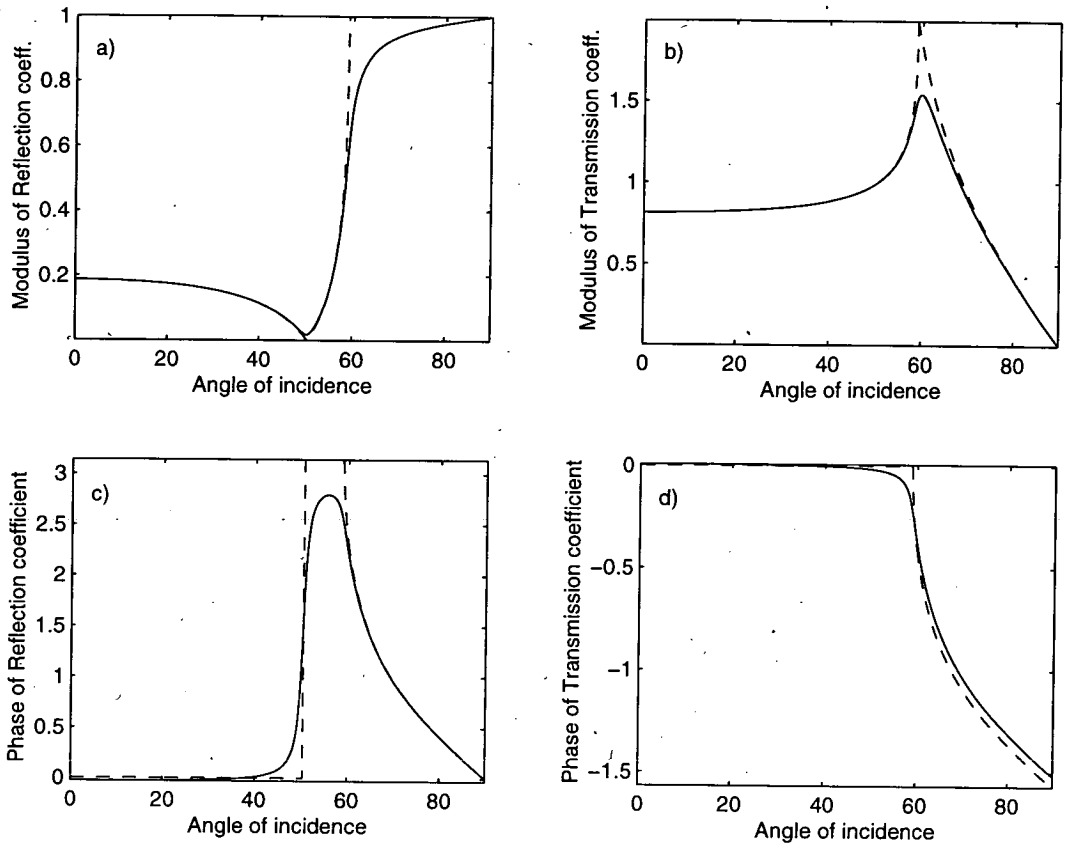

Figure 5.1. Reflection coefficients for SH-wave, modulus and phase. a) Amplitude of Reflected wave. b) Amplitude of Transmitted wave. c) Phase of Reflected wave. d) Phase of Transmitted wave. Solid line: poroelastic case; Dashed line: elastic case.

To plot figure 5.1 I have computed reflection coefficients for regularly spaced angles of incidence for a homogeneous incident plane wave (i.e. real angles of incidence). In this case ς is real but the horizontal slowness q is not necessarily real and is actually given by :

$$q = \sin(i) * \sqrt{X}$$

where i is the angle of incidence, X is the square of the slowness obtained from the dispersion equation (5.7) and its square root is chosen such that its real part is positive and imaginary part is negative.

The main difference between poroelastic and elastic cases can be observed only for post-critical angles of incidence where the amplitude of reflected wave is noticeably lower than in elastic case. An illuminating discussion of total internal reflection of S_H waves can be found in Hudson [1962].

5.4 Reflection matrix for P-, S-, Biot waves

We can formalise boundary conditions (5.4) introducing a 6-vector containing the continuous components of wave field:

$$F = (u_z, \quad \sigma_{xz}, \quad \dot{\xi}_z, \quad u_x, \quad \sigma_{zz}, \quad P)^T \tag{5.17}$$

where I have ignored for a while the pressure drop caused by partially sealed interface ($\kappa_s = \infty$). Let $\grave{F}^{\alpha}_{1,2}$ and $\acute{F}^{\alpha}_{1,2}$ be 6-vectors for downgoing and upgoing waves, of the type $\alpha = P$-, $S(S_V)$-, Biot-wave, in the first (upper) and second (lower) medium correspondingly. Then the boundary conditions (5.4) for the twelve downgoing and upgoing components of the P-, $Biot$- and S-waves can be formally written as:

$$\begin{aligned} &\grave{F}^P_1 \cdot \grave{P}_1 + \grave{F}^B_1 \cdot \grave{B}_1 + \grave{F}^S_1 \cdot \grave{S}_1 + \acute{F}^P_1 \cdot \acute{P}_1 + \acute{F}^B_1 \cdot \acute{B}_1 + \acute{F}^S_1 \cdot \acute{S}_1 \\ &= \acute{F}^P_2 \cdot \acute{P}_2 + \acute{F}^B_2 \cdot \acute{B}_2 + \acute{F}^S_2 \cdot \acute{S}_2 + \grave{F}^P_2 \cdot \grave{P}_2 + \grave{F}^B_2 \cdot \grave{B}_2 + \grave{F}^S_2 \cdot \grave{S}_2 \end{aligned} \tag{5.18}$$

where $\acute{P}_{1,2}$, $\acute{B}_{1,2}$ are $\acute{S}_{1,2}$ with an acute accent are the amplitudes of upgoing components and $\grave{P}_{1,2}$, $\grave{B}_{1,2}$ are $\grave{S}_{1,2}$ with a grave accent are the amplitudes of downgoing components of respectively P-wave, Biot-wave and S-wave in either 1^{st} or 2^{nd} medium.

Collecting terms in equation (5.18) with upgoing components in first medium and downgoing components in the second medium on the LHS, and collecting terms with downgoing components in the first medium and upgoing components in the second medium on the RHS, we can rewrite equation (5.18) in the following way:

$$\begin{aligned} &\acute{F}^P_1 \cdot \acute{P}_1 + \acute{F}^B_1 \cdot \acute{B}_1 + \acute{F}^S_1 \cdot \acute{S}_1 - \grave{F}^P_2 \cdot \grave{P}_2 - \grave{F}^B_2 \cdot \grave{B}_2 - \grave{F}^S_2 \cdot \grave{S}_2 \\ &= -\grave{F}^P_1 \cdot \grave{P}_1 - \grave{F}^B_1 \cdot \grave{B}_1 - \grave{F}^S_1 \cdot \grave{S}_1 + \acute{F}^P_2 \cdot \acute{P}_2 + \acute{F}^B_2 \cdot \acute{B}_2 + \acute{F}^S_2 \cdot \acute{S}_2 \end{aligned} \tag{5.19}$$

This equation can be presented in matrix form:

$$[\acute{F}^P_1 \quad \acute{F}^B_1 \quad \acute{F}^S_1 \quad -\grave{F}^P_2 \quad -\grave{F}^B_2 \quad -\grave{F}^S_2] \begin{pmatrix} \acute{P}_1 \\ \acute{B}_1 \\ \acute{S}_1 \\ \grave{P}_2 \\ \grave{B}_2 \\ \grave{S}_2 \end{pmatrix} = [-\grave{F}^P_1 \quad -\grave{F}^B_1 \quad -\grave{F}^S_1 \quad \acute{F}^P_2 \quad \acute{F}^B_2 \quad \acute{F}^S_2] \begin{pmatrix} \grave{P}_1 \\ \grave{B}_1 \\ \grave{S}_1 \\ \acute{P}_2 \\ \acute{B}_2 \\ \acute{S}_2 \end{pmatrix} \tag{5.20}$$

where $[\acute{F}^P \quad \acute{F}^B \quad \acute{F}^S \quad -\grave{F}^P \quad -\grave{F}^B \quad -\grave{F}^S]$ and $[-\grave{F}^P_1 \quad -\grave{F}^B_1 \quad -\grave{F}^S_1 \quad \acute{F}^P_2 \quad \acute{F}^B_2 \quad \acute{F}^S_2]$ are 6×6 matrices with columns given by 6-vectors F.

The amplitude vector $(\acute{P}_1 \quad \acute{B}_1 \quad \acute{S}_1 \quad \grave{P}_2 \quad \grave{B}_2 \quad \grave{S}_2)^T$ on the LHS of equation (5.21) represents a field emergent from the interface (in medium 1 and 2) while the amplitude vector $(\grave{P}_1 \quad \grave{B}_1 \quad \grave{S}_1 \quad \acute{P}_2 \quad \acute{B}_2 \quad \acute{S}_2)^T$ on the RHS of equation (5.21) represents an incident field (in medium 1 and 2).

When the amplitude vector $(\grave{P}_1 \quad \grave{B}_1 \quad \grave{S}_1 \quad \acute{P}_2 \quad \acute{B}_2 \quad \acute{S}_2)^T$ on the left-hand side of equation (5.21) is set to $(1 \quad 0 \quad 0 \quad 0 \quad 0 \quad 0)^T$, equation (5.21) yields:

$$[\acute{F}_1^P \quad \acute{F}_1^B \quad \acute{F}_1^S \quad -\grave{F}_2^P \quad -\grave{F}_2^B \quad -\grave{F}_2^S] \begin{pmatrix} R_{\grave{P}\acute{P}} \\ R_{\grave{P}\acute{B}} \\ R_{\grave{P}\acute{S}} \\ T_{\grave{P}\grave{P}} \\ T_{\grave{P}\grave{B}} \\ T_{\grave{P}\grave{S}} \end{pmatrix} = -\grave{F}_1^P \tag{5.21}$$

where $R_{\alpha\beta}$ and $T_{\alpha\beta}$ are reflection and transmission coefficients of a wave of type α into a wave of type β. For instance $R_{\grave{P}\acute{S}}$ is the reflection coefficient for a P-wave incident from the upper medium and reflected (and converted) into a Biot slow wave in the upper medium.

Similarly, when the amplitude vector $(\grave{P}_1 \quad \grave{B}_1 \quad \grave{S}_1 \quad \acute{P}_2 \quad \acute{B}_2 \quad \acute{S}_2)^T$ on the RHS of equation (5.21) is set to $(0 \quad 1 \quad 0 \quad 0 \quad 0 \quad 0)^T$, equation (5.21) yields:

$$[\acute{F}_1^P \quad \acute{F}_1^B \quad \acute{F}_1^S \quad -\grave{F}_2^P \quad -\grave{F}_2^B \quad -\grave{F}_2^S] \begin{pmatrix} R_{\grave{B}\acute{P}} \\ R_{\grave{B}\acute{B}} \\ R_{\grave{B}\acute{S}} \\ T_{\grave{B}\grave{P}} \\ T_{\grave{B}\grave{B}} \\ T_{\grave{B}\grave{S}} \end{pmatrix} = -\grave{F}_1^B \tag{5.22}$$

Repeating this substitution for all other elements, I obtain equations for all the reflection-transmission coefficients at the interface. These equations can be gathered in one matrix equation:

$$\left[\acute{F}_1^P \acute{F}_1^B \acute{F}_1^S - \grave{F}_2^P - \grave{F}_2^B - \grave{F}_2^S\right] \begin{bmatrix} R_{\grave{P}\acute{P}} & R_{\grave{B}\acute{P}} & R_{\grave{S}\acute{P}} & T_{\acute{P}\acute{P}} & T_{\acute{B}\acute{P}} & T_{\acute{S}\acute{P}} \\ R_{\grave{P}\acute{B}} & R_{\grave{B}\acute{B}} & R_{\grave{S}\acute{B}} & T_{\acute{P}\acute{B}} & T_{\acute{B}\acute{B}} & T_{\acute{S}\acute{B}} \\ R_{\grave{P}\acute{S}} & R_{\grave{B}\acute{S}} & R_{\grave{S}\acute{S}} & T_{\acute{P}\acute{S}} & T_{\acute{B}\acute{S}} & T_{\acute{S}\acute{S}} \\ T_{\grave{P}\grave{P}} & T_{\grave{B}\grave{P}} & T_{\grave{S}\grave{P}} & R_{\acute{P}\grave{P}} & R_{\acute{B}\grave{P}} & R_{\acute{S}\grave{P}} \\ T_{\grave{P}\grave{B}} & T_{\grave{B}\grave{B}} & T_{\grave{S}\grave{B}} & R_{\acute{P}\grave{B}} & R_{\acute{B}\grave{B}} & R_{\acute{S}\grave{B}} \\ T_{\grave{P}\grave{S}} & T_{\grave{B}\grave{S}} & T_{\grave{S}\grave{S}} & R_{\acute{P}\grave{S}} & R_{\acute{B}\grave{S}} & R_{\acute{S}\grave{S}} \end{bmatrix} = [-\grave{F}_1^P - \grave{F}_1^B - \grave{F}_1^S \acute{F}_2^P \acute{F}_2^B \acute{F}_2^S] \tag{5.23}$$

Using the results of Chapter 4 summarised in tables (4.1-4.4), all components of F vectors can be explicitly determined in equation (5.17). Equation (5.23) can be presented in the simple block-matrix form:

$$\begin{pmatrix} P_1 & P_2 \\ Q_1 & -Q_2 \end{pmatrix} \begin{pmatrix} R_{11} & T_{21} \\ T_{12} & R_{22} \end{pmatrix} = \begin{pmatrix} P_1 & P_2 \\ -Q_1 & Q_2 \end{pmatrix} \tag{5.24}$$

To achieve this presentation I have introduced the following block-matrices:

$$P = \begin{pmatrix} p & b & 1 \\ 2\mu p & 2\mu b & \mu(1-s^2) \\ R_P p & R_B b & R_S \end{pmatrix} L \tag{5.25}$$

and

$$Q = \begin{pmatrix} -1 & -1 & s \\ -(1+p^2)(H - R_P C) + 2\mu & -(1+b^2)(H - R_B C) + 2\mu & -2\mu s \\ -(1+p^2)(MR_P - C)q & -(1+b^2)(MR_B - C)q & 0 \end{pmatrix} L \tag{5.26}$$

where

$$L = \begin{pmatrix} \frac{1}{\sqrt{1+p^2}} & 0 & 0 \\ 0 & \frac{1}{\sqrt{1+b^2}} & 0 \\ 0 & 0 & \frac{1}{\sqrt{1+s^2}} \end{pmatrix} \tag{5.27}$$

Indices 1 and 2 in block-matrix equation (5.24) refer to the medium above and below the interface respectively.

The block-matrix $R_{11} = \begin{bmatrix} R_{\grave{P}\acute{P}} & R_{\grave{B}\acute{P}} & R_{\grave{S}\acute{P}} \\ R_{\grave{P}\acute{B}} & R_{\grave{B}\acute{B}} & R_{\grave{S}\acute{B}} \\ R_{\grave{P}\acute{S}} & R_{\grave{B}\acute{S}} & R_{\grave{S}\acute{S}} \end{bmatrix}$ which appears in the top-left quarter of the second matrix on the LHS of equations (5.24) and (5.23) contains all reflection-conversion coefficients for a wave emerging in the first medium after reflection of a wave incident on the interface in the first medium. Similarly, R_{22} in the bottom-right quarter of the second matrix on the LHS of equations (5.23) and (5.24) gathers the reflection-conversion coefficients for a wave emerging in medium 2 from a wave incident the interface from medium 2. T_{12} in the bottom-left quarter contains the transmission-conversion coefficients for waves emergent in second medium from waves incident in first medium and T_{21} in the top-right quarter contains the transmission-conversion coefficients for waves emergent in first medium from waves incident in second medium.

Equations (5.24-5.27) provide all the reflection and transmission coefficients at the interface between two-fluid-saturated-poro–elastic solids. These equations can also be applied for specific

situations of the interface between poroelastic and liquid half-spaces and poroelastic and elastic half-spaces.

I can further simplify matrix equation (5.24) to derive its solution in a convenient block-matrix form:

$$\begin{pmatrix} I & I \\ Q_1P_1^{-1} & -Q_2P_2^{-1} \end{pmatrix}\begin{pmatrix} P_1 & 0 \\ 0 & P_2 \end{pmatrix}\begin{pmatrix} R_{11} & T_{21} \\ T_{12} & R_{22} \end{pmatrix} = \begin{pmatrix} I & I \\ -Q_1P_1^{-1} & Q_2P_2^{-1} \end{pmatrix}\begin{pmatrix} P_1 & 0 \\ 0 & P_2 \end{pmatrix}$$

or equally:

$$\begin{pmatrix} P_1 & 0 \\ 0 & P_2 \end{pmatrix}\begin{pmatrix} R_{11} & T_{21} \\ T_{12} & R_{22} \end{pmatrix}\begin{pmatrix} P_1 & 0 \\ 0 & P_2 \end{pmatrix}^{-1} = \begin{pmatrix} I & I \\ Q_1P_1^{-1} & -Q_2P_2^{-1} \end{pmatrix}^{-1}\begin{pmatrix} I & I \\ -Q_1P_1^{-1} & Q_2P_2^{-1} \end{pmatrix}$$

The inverse matrix on RHS of this equation is given by:

$$\begin{pmatrix} I & I \\ Q_1P_1^{-1} & -Q_2P_2^{-1} \end{pmatrix}^{-1} = [Q_1P_1^{-1} + Q_2P_2^{-1}]^{-1}\begin{pmatrix} Q_2P_2^{-1} & 1 \\ Q_1P_1^{-1} & -1 \end{pmatrix} \tag{5.28}$$

This yields the solution of equation (5.24):

$$\begin{pmatrix} R_{11} & T_{21} \\ T_{12} & R_{22} \end{pmatrix} = \begin{pmatrix} P_1^{-1} & 0 \\ 0 & P_2^{-1} \end{pmatrix}\left\{[Q_1P_1^{-1} + Q_2P_2^{-1}]^{-1}\begin{pmatrix} Q_2P_2^{-1} & 1 \\ Q_1P_1^{-1} & -1 \end{pmatrix} \times \begin{pmatrix} I & I \\ -Q_1P_1^{-1} & Q_2P_2^{-1} \end{pmatrix}\right\}\begin{pmatrix} P_1 & 0 \\ 0 & P_2 \end{pmatrix} \tag{5.29}$$

and the block-elements of the reflection matrix are:

$$\begin{aligned} R_{11} &= P_1^{-1}[Q_1P_1^{-1} + Q_2P_2^{-1}]^{-1}(Q_2P_2^{-1} - Q_1P_1^{-1})P_1 \\ T_{12} &= P_2^{-1}[Q_1P_1^{-1} + Q_2P_2^{-1}]^{-1}(2Q_1) \\ R_{22} &= P_2^{-1}[Q_1P_1^{-1} + Q_2P_2^{-1}]^{-1}(Q_1P_1^{-1} - Q_2P_2^{-1})P_2 \\ T_{21} &= P_1^{-1}[Q_1P_1^{-1} + Q_2P_2^{-1}]^{-1}(2Q_2) \end{aligned} \tag{5.30}$$

From equation (5.24) or (5.30) the reflection/transmission coefficients matrix can be computed numerically.

When the effect of interfacial permeability transmissivity [Deresiewicz and Skalak, 1963; Bourbie et al., 1986] (described by coefficient κ_s in equation (3.2) for the fluid-pressure drop through a horizontal interface) is taken into account, we can define 6-vector F in the following way:

$$F_1 = F^- = (u_z, \quad \sigma_{xz}, \quad \dot{\xi}_z, \quad u_x, \quad \sigma_{zz}, \quad P - \tfrac{\dot{\xi}_z}{2\kappa_s})^T \tag{5.31}$$

for the upper medium (medium 1) and, correspondingly:

$$F_2 = F^+ = (u_z, \quad \sigma_{xz}, \quad \dot{\xi}_z, \quad u_x, \quad \sigma_{zz}, \quad P + \tfrac{\dot{\xi}_z}{2\kappa_s})^T \tag{5.32}$$

for the lower medium.

Following line by line our previous derivation of reflection/transmission coefficients in equations (5.18-5.24), we can generalise the final result given by equation (5.24) in the following form:

$$\begin{pmatrix} P_1 & P_2 \\ Q_1^- & -Q_2^- \end{pmatrix} \begin{pmatrix} R_{11} & T_{21} \\ T_{12} & R_{22} \end{pmatrix} = \begin{pmatrix} P_1 & P_2 \\ -Q_1^+ & Q_2^+ \end{pmatrix} \tag{5.33}$$

where

$$P = \begin{pmatrix} p & b & 1 \\ 2\mu p & 2\mu b & \mu(1-s^2) \\ R_P p & R_B b & R_S \end{pmatrix} L, \quad \text{with} \quad L = \begin{pmatrix} \frac{1}{\sqrt{1+p^2}} & 0 & 0 \\ 0 & \frac{1}{\sqrt{1+b^2}} & 0 \\ 0 & 0 & \frac{1}{\sqrt{1+s^2}} \end{pmatrix}$$

and

$$Q^+ = \begin{pmatrix} -1 & -1 & s \\ -(1+p^2)(H - R_P C) + 2\mu & -(1+b^2)(H - R_B C) + 2\mu & -2\mu s \\ -(1+p^2)(MR_P - C)q \pm \frac{R_P p}{2\kappa_s} & -(1+b^2)(MR_B - C)q \pm \frac{R_B b}{2\kappa_s} & 0 \end{pmatrix} L$$

The solutions of (5.33) can then be written:

$$\begin{aligned} R_{11} &= P_1^{-1}[Q_1^- P_1^{-1} + Q_2^- P_2^{-1}]^{-1}(Q_2^+ P_2^{-1} - Q_1^+ P_1^{-1})P_1 \\ T_{21} &= 2P_2^{-1}[Q_1^- P_1^{-1} + Q_2^- P_2^{-1}]^{-1} Q_1^+ \\ R_{22} &= P_2^{-1}[Q_1^- P_1^{-1} + Q_2^- P_2^{-1}]^{-1}(Q_1^+ P_1^{-1} - Q_2^+ P_2^{-1})P_2 \\ T_{12} &= 2P^{-1}[Q_1^- P_1^{-1} + Q_2^- P_2^{-1}]^{-1} Q_2^+ \end{aligned} \tag{5.34}$$

or in terms of the symmetrised matrix $Q = (Q^+ + Q^-)/2$:

$$\begin{aligned} R_{11} &= P_1^{-1}[Q_1 P_1^{-1} + Q_2 P_2^{-1} - \Delta]^{-1}(Q_2 P_2^{-1} - Q_1 P_1^{-1})P_1 \\ T_{12} &= P_2^{-1}[Q_1 P_1^{-1} + Q_2 P_2^{-1} - \Delta]^{-1}(2Q_1 P_1^{-1} + \Delta)P_1 \\ R_{22} &= P_2^{-1}[Q_1 P_1^{-1} + Q_2 P_2^{-1} - \Delta]^{-1}(Q_1 P_1^{-1} - Q_2 P_2^{-1})P_2 \\ T_{21} &= P_1^{-1}[Q_1 P_1^{-1} + Q_2 P_2^{-1} - \Delta]^{-1}(2Q_2 P_2^{-1} + \Delta)P_2 \end{aligned} \tag{5.35}$$

where

$$\Delta = \frac{1}{\kappa_s} \begin{pmatrix} 0 & 0 & 0 \\ 0 & 0 & 0 \\ 2R_S & 2R_S & 1 \end{pmatrix} \tag{5.36}$$

Note that the solution given by (5.35) looks very similar to the solution for the reflection and transmission coefficients in conventional viscoelasticity [Kennett 1983, Graebner 1992].

5.5 Summary

In this chapter I have introduced a general set of boundary conditions at the horizontal interface between two fluid-saturated poroelastic media following Deresiewicz and Skalak [1963] approach based on extended Newmann's uniqueness theorem. Substituting the wave-field decomposition derived in the previous chapter (tables 4.1-4.4) into the boundary conditions, I have derived matrix equations for reflection/transmission coefficients for all types of waves.

The reflection and transmission coefficients for S_H-wave are decoupled from reflection/transmission coefficients of all other waves and are given by matrix equation (5.15). In figure 5.1 I have shown a simple numerical solution for S_H reflection where critical angle is present. The main result however is given by matrix equation (5.24) coupling reflection and transmission coefficients for P-waves, Biot waves and S_V waves. The extended form of (5.24) is given by matrix equation (5.33) for the case when effect of partially sealed interface is taken in to account.

Matrix equations (5.15) for S_H-wave and (5.24) and (5.33) for P-, Biot and S_V-waves completely solve the reflection problem of plane harmonic waves in fluid-saturated poroelastic media.

Chapter 6

NUMERICAL ALGORITHM

6.1 Introduction

The algorithm for computing reflection and transmission coefficients in isotropic fluid-saturated poroelastic media is given by equations (5.15) and (5.24) together with dispersion equations (3.14) and (3.29) for S_H-waves and for P-, Biot and S_V-waves respectively. For a given frequency ω and horizontal slowness q, I can find vertical slownesses for all types of waves interacting at the interface. I choose the imaginary part of vertical slowness in a way to guarantee attenuation of inhomogeneous waves at the infinite distance from the interface.

In this chapter I test my algorithm comparing it with the results calculated by means of purely elastic algorithm [Aki and Richards 1980]. I artificially supress the effect caused the relative motion of pore-fluid (Biot wave) on the reflection and transmission of seismic waves by choosing relatively low values of permeability and frequency. To demonstrate the effect of viscoelastic attenuation in my algorithm I introduce imaginary corrections to the elastic moduli K_B and μ.

6.2 Viscoelastic approximation

To test my numerical algorithm, I consider an interface between two isotropic half-spaces. Table (6.1a) specifies the parameters of the elastic half-spaces, considered as a reference model. Table (6.1b) specifies the physical parameters of poroelastic half-spaces. Note that the velocities specified in Table 6.1a are zero-frequency asymptotic values (given by Gassmann's equations (2.28)) for poroelastic media with parameters given in table 6.1b.

Table 6.1a

Elastic	*Medium 1*	*Medium 2*
V_P (Km/s)	2.36	2.80
V_S (Km/s)	1.22	1.42
ρ $(g.cm^{-3})$	1.92	2.44

Table 6.1b

Poroelastic	*Medium 1*	*Medium 2*
K_r (GPa)	8.66	16.0
ρ_r $(g.cm^{-3})$	2.0	2.5
K_f (GPa)	2.0	2.0
ρ_f $(g.cm^{-3})$	1.0	1.0
η (cP)	0.01	0.01
K_b (GPa)	0.044	0.8
μ (GPa)	2.88	4.9
ϕ	0.08	0.04
c	1.25	1.25
k (cm^2)	$1 \quad 10^{-8}$	$0.1 \; 10^{-8}$
δ	0.01	0.01
ω_B	$8 \quad 10^4$	$4 \quad 10^5$

In order to suppress the physical effects caused by wave-induced pore-fluid flow (Biot wave), I choose in this particular case only low frequency of seismic waves and relatively low permeability and porosity. The effect of viscoelasticity is simulated by adding imaginary parts to moduli K_B and μ. Parameter $\delta = \pi/Q$, where Q is a quality factor ($Q \gg 1$), is responsible for viscoelastic attenuation of P- and S-waves and is defined as [Aki and Richards 1980]:

$$\delta = \pi \frac{Im(K_b)}{Re(K_b)} = \pi \frac{Im(\mu)}{Re(\mu)} \tag{6.1}$$

Figure (6.1) shows the behaviour of reflection coefficients $R_{\dot{P}\dot{P}}$ and $R_{\dot{P}\dot{S}}$ for incident P-wave simulated by my poroelastic algorithm.

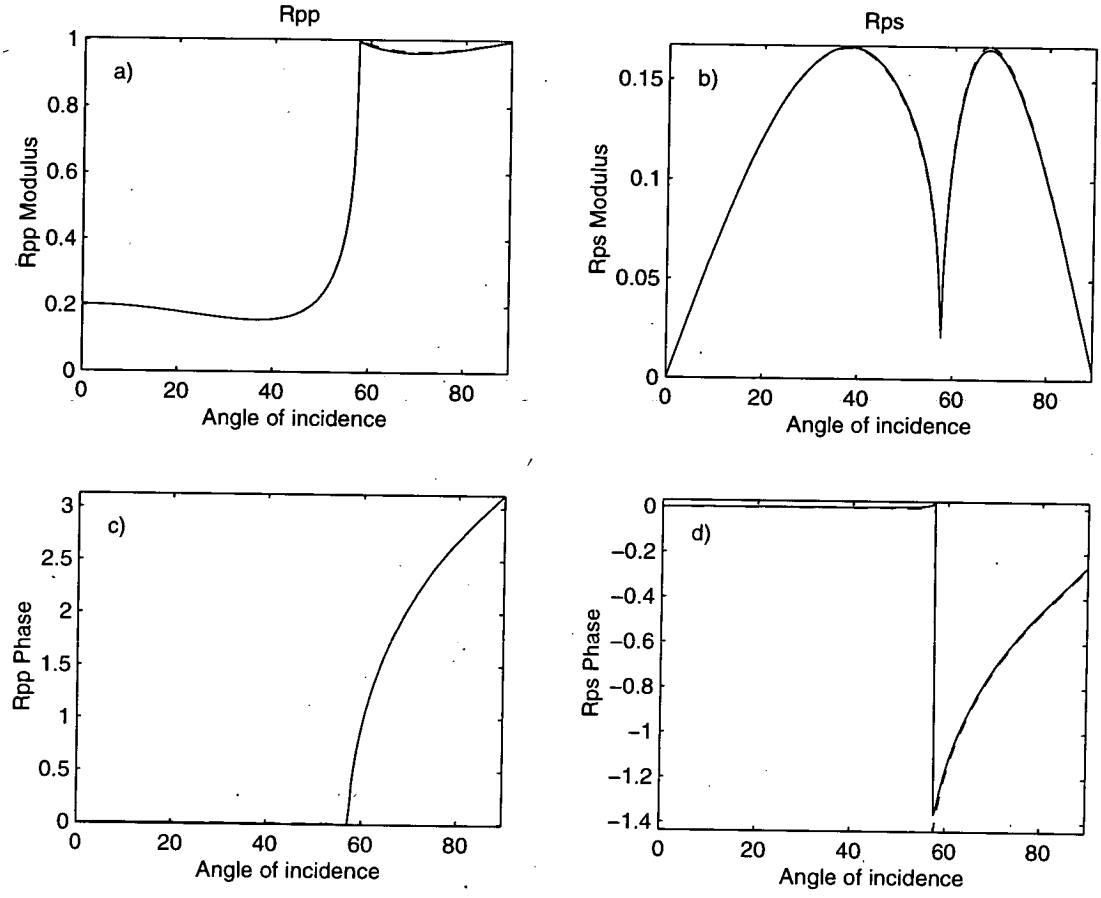

Figure 6.1. Reflection coefficients for viscoelastic media simulated by my poroelastic algorithm. a) Amplitude of reflection coefficient $R_{\dot{P}\dot{P}}$. b) Amplitude of reflection coefficient $R_{\dot{P}\dot{S}}$. c) Phase of coefficient for reflection of $R_{\dot{P}\dot{P}}$. d) Phase of coefficient for conversion of $R_{\dot{P}\dot{S}}$. Dashed line is elastic model ($\delta \approx 0$); Solid line is my poroelastic algorithm with ($Q = 314$).

Dashed lines in Figure 6.1 correspond to the elastic algorithm as given by Aki and Richards [1980] and my numerical results for very low frequency and $\delta = 0$. The results of my poroelastic algorithm are indistinguishable from the results given by Aki and Richards' elastic algorithm. Solid curves in figure 6.1 show the effect of viscoelasticity when imaginary parts of complex shear wave moduli μ and skeleton bulk moduli K_b are non-zero. Physical effects of Biot-wave are suppressed by low chosen frequency $f = \frac{\omega}{2\pi} = 1.6KHz$ and low values of permeability and porosity in my model (table 6.1b).

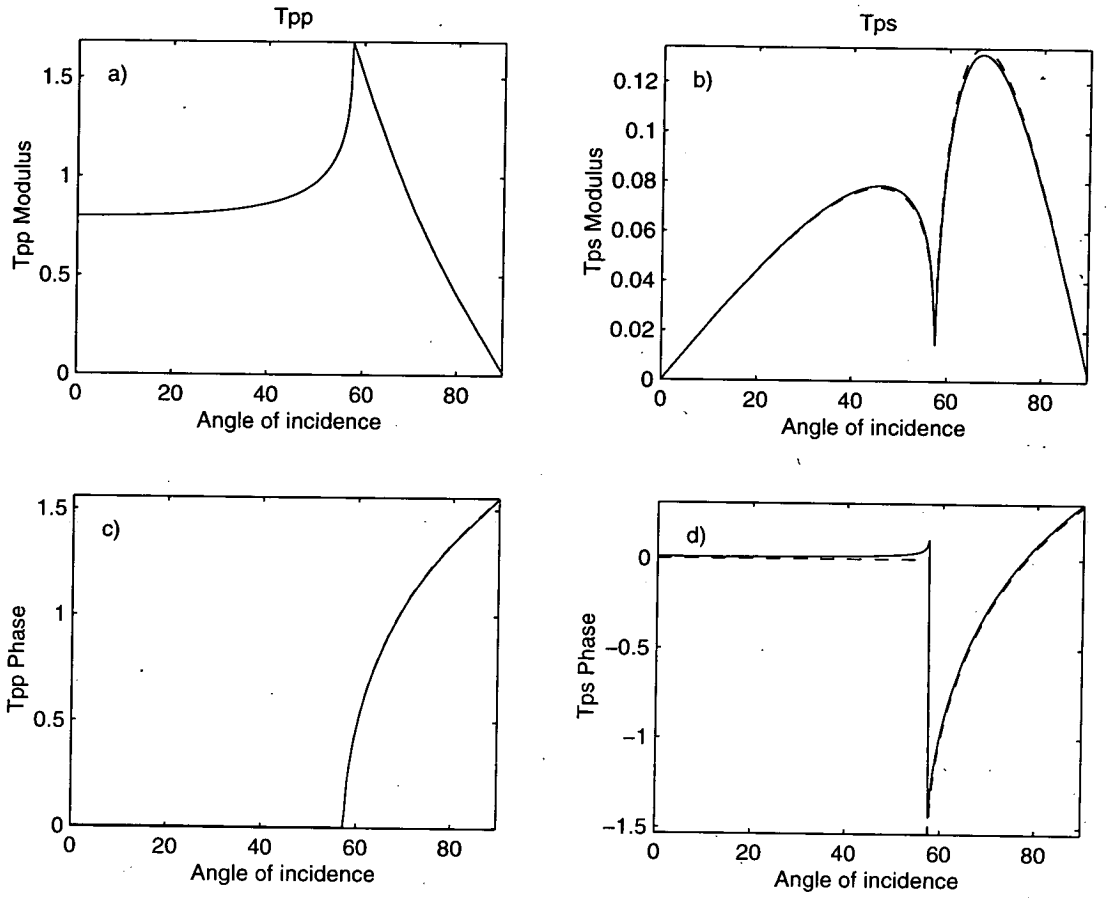

Figure 6.2. Transmission coefficients for viscoelastic media simulated by my poroelastic algorithm. a) Amplitude of tranmission coefficient $T_{\dot{P}\dot{P}}$. b) Amplitude of transmission coefficient $T_{\dot{P}\dot{S}}$. c) Phase of coefficient for transmission of $T_{\dot{P}\dot{P}}$. d) Phase of coefficient for transmission of $T_{\dot{P}\dot{S}}$. Dashed line is elastic model ($\delta \approx 0$); Solid line is my poroelastic algorithm with ($Q = 314$).

Dashed lines in Figure 6.2 correspond to the elastic algorithm as given by Aki and Richards [1980] and my numerical results for very low frequency and $\delta = 0$. The results of my poroelastic algorithm are indistinguishable from the results given by Aki and Richards' elastic algorithm. Solid curves in figure 6.2 shows the effect of visco-elasticity when imaginary parts of complex shear wave moduli μ and skeleton bulk moduli K_b are non-zero. Physical effects of Biot-wave are suppressed by very low chosen frequency $f = \frac{\omega}{2\pi} = 1.6KHz$.

Next figures 6.3 and 6.4 show reflection and transmission coefficients for incident S_V-wave (the case of incident S_H-wave has been demonstrated in figure 5.1 in chapter 5).

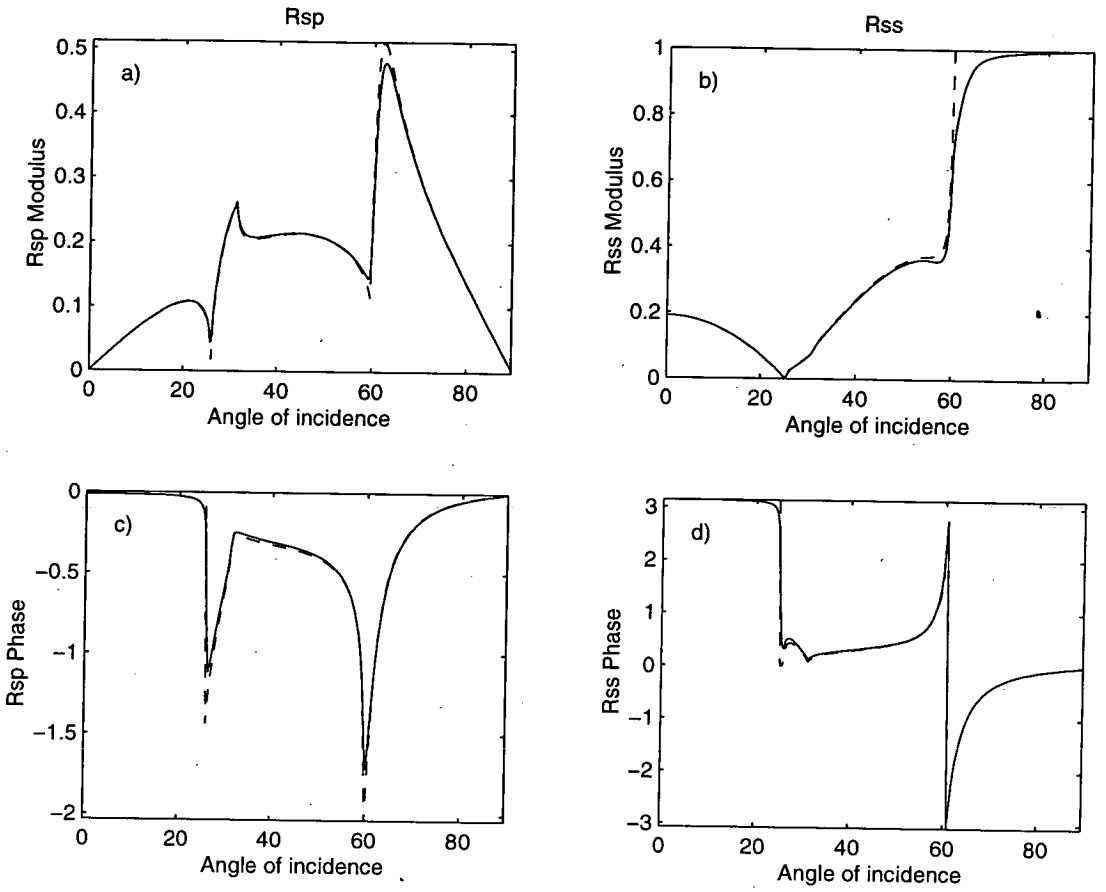

Figure 6.3. Reflection coefficients for viscoelastic media simulated by my poroelastic algorithm. a) Amplitude of reflection coefficient $R_{\dot{S}\acute{P}}$ b) Amplitude of reflection coefficient $R_{\dot{S}\acute{S}}$ c) Phase of reflection coefficient $R_{\dot{S}\acute{P}}$ d) Phase of reflection coefficient $R_{\dot{S}\acute{S}}$ Solid line is my poroelastic model. Dashed line is elastic reference model.

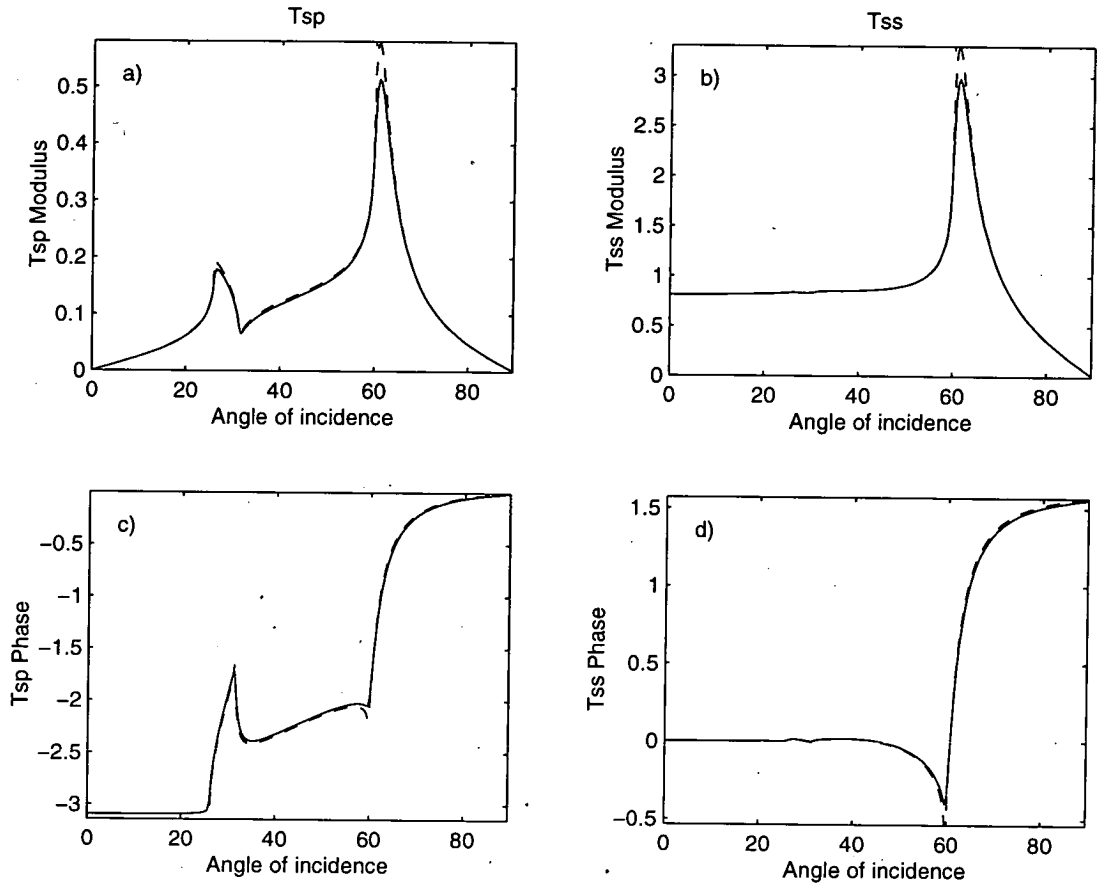

Figure 6.4. Transmission coefficients for viscoelastic media simulated by my poroelastic algorithm. a) Amplitude of transmission coefficient $T_{\dot{S}\dot{P}}$ b) Amplitude of transmission coefficient $T_{\dot{S}\dot{S}}$ c) Phase of transmission coefficient $T_{\dot{S}\dot{P}}$ d) Phase of transmission coefficient $T_{\dot{S}\dot{S}}$ Solid line is my poroelastic model. Dashed line is elastic reference model.

Figures 6.1 to 6.4 clearly show that my algorithm is in excellent agreement with an elastic reference algorithm of Aki and Richards [1980]. The correction from the elastic case for my reflection and transmission coefficients computed with my poroelastic algorithm in the viscoelastic limit are physically sensible and my reflection coefficients show a behaviour similar to the behaviour of reflection coefficients invistigated by Bourbie and Gonzales-Serrano [1983] with purely viscoelastic algorithm (no pore fluid involved).

6.3 Summary

Considering the complexity of the phenomena involved in the test model (including two critical angles for incident S_V-wave) my algorithm could have easily led to unstable or unphysical results. I have therefore successfully tested my poroelastic algorithm in the (visco-)elastic limit and have observed an excellent agreement.

Chapter 7

FREQUENCY DEPENDENT POROELASTIC REFLECTIONS AT DIFFERENT ANGLES OF INCIDENCE

7.1 Introduction

In the previous chapter, I have tested the developed poroelastic algorithm with respect to the elastic model. In the following sections I apply my algorithm to investigate the effects caused by fluid motion in poroelastic permeable matrix. I first consider the variations of reflection coefficients with respect to the angle of incidence (at reference frequencies) and then the variations of the coefficients with frequency (at given angles of incidence).

7.2 Poroelastic effects at different frequencies.

In this section I investigate frequency-dependent behaviour of reflection coefficients at the interface between two poroelastic media with physical parameters specified in table 7.1.

Table 7.1

	Top	*Bottom*
K_r (GPa)	8.66	16.0
ρ_r $(g.cm^{-3})$	2.0	2.5
K_f (GPa)	2.0	2.0
ρ_f $(g.cm^{-3})$	1.0	1.0
η (cP)	0.01	0.01
K_b (GPa)	0.044	0.8
μ (GPa)	2.88	4.9
ϕ	0.2	0.04
c	1.25	1.25
k (cm^2)	$1.\ 10^{-8}$	$0.1\ 10^{-8}$
δ	0.005	0.005
f_{Biot} (Hz)	$32\ \ 10^3$	$64\ \ 10^3$

In this model I have two different Biot-frequencies: $32KHz$ for the top medium and $64KHz$ for the bottom one. The top medium is a high porosity medium with relatively low P- and S-waves velocities. The bottom medium has essentially smaller values of porosity and permeability and relatively high seismic velocities. As a consequence I have one critical angle for incident P-wave and two critical angles for incident shear wave. Figures 7.1-7.8 show the behaviour of all possible reflection coefficients (R_{PP},R_{PS},R_{PB}) as a function of angle of incidence for four different values of frequency.

Figures 7.1 and 7.2 present a low frequency case with $f = 3.2KHz$, ten times smaller than the lowest Biot frequency. It clearly demonstrates that the results are very close to that of Gassmann's approximation (elastic algorithm). The main difference can be seen only in the vicinity of second critical angle for R_{SP} and R_{SS} reflection coefficients. Figures 7.3 to 7.6 show reflection coefficients when the frequency of incident wave is equal to the lowest Biot-frequency $f = 32KHz$ (top medium) and highest Biot-frequency $f = 64KHz$ (bottom medium). To conclude, figures 7.7 and 7.8 show the behaviour of reflection coefficients at the very high frequency of $f = 640KHz$, higher than any of the two Biot frequencies involved in the model.

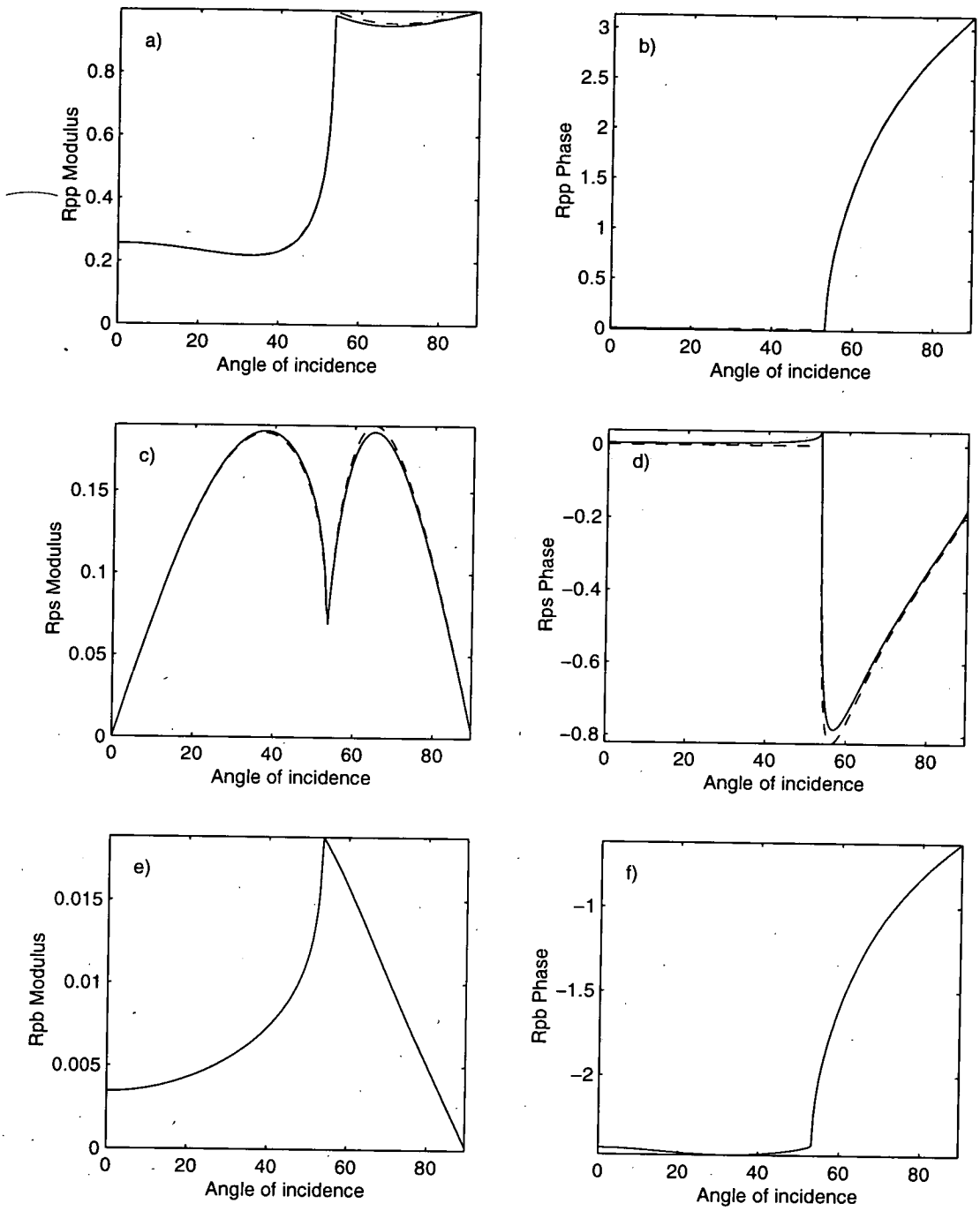

Figure 7.1. Dependence of reflection coefficients on the angle of incidence for poroelastic media at low frequency $f = 3.2KHz$, P-wave incident. a) and b) $R_{\dot{P}\dot{P}}$ amplitude and phase. c) and d) $R_{\dot{P}\dot{S}}$ amplitude and phase. e) and f) $R_{\dot{P}\dot{B}}$ amplitude and phase. Solid curves: poroelastic model with parameters from table 7.1. Dashed curves: Gassmann's zero-frequency approximation (elastic algorithm).

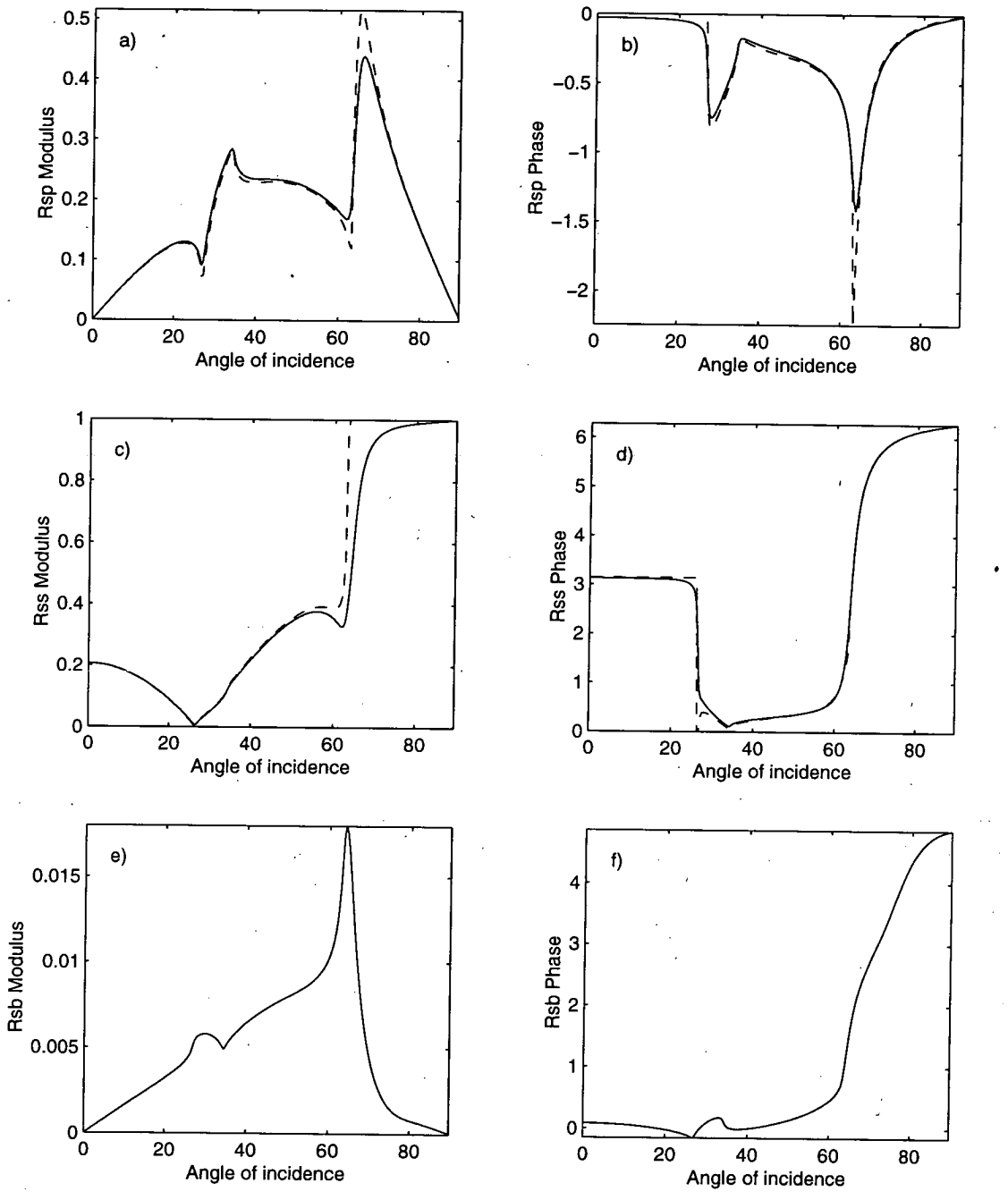

Figure 7.2. Dependence of reflection coefficients on the angle of incidence for poroelastic media at low frequency $f = 3.2KHz$, S-wave incident. a) and b) $R_{\hat{S}\hat{P}}$ amplitude and phase. c) and d) $R_{\hat{S}\hat{S}}$ amplitude and phase. e) and f) $R_{\hat{S}\hat{B}}$ amplitude and phase. Solid curves: poroelastic model with parameters from table 7.1. Dashed curves: Gassmann's zero-frequency approximation.

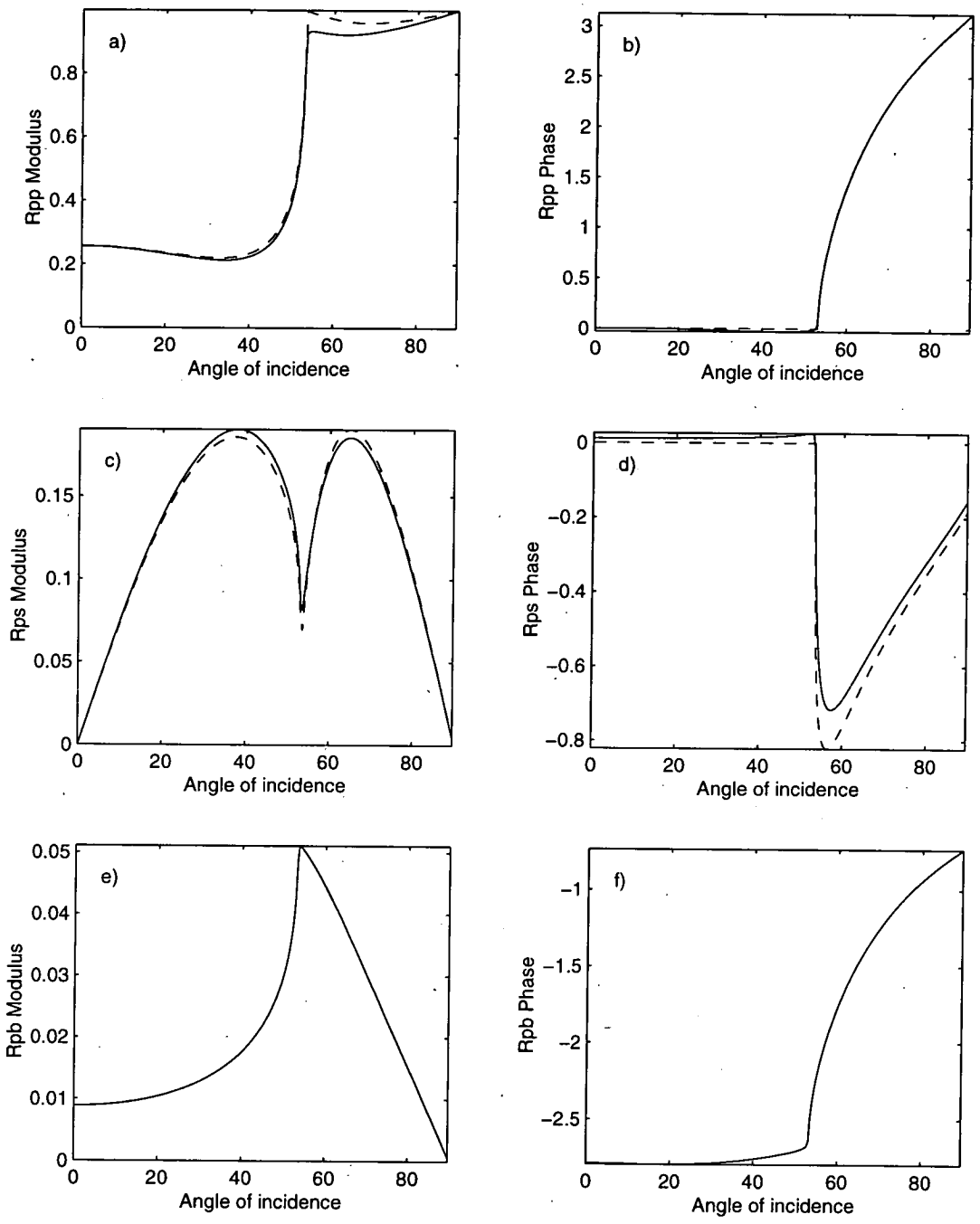

Figure 7.3. Dependence of reflection coefficients on the angle of incidence for poroelastic media at frequency $f = 32KHz$, P-wave incident. a) and b) $R_{\dot{P}\dot{P}}$ amplitude and phase. c) and d) $R_{\dot{P}\dot{S}}$ amplitude and phase. e) and f) $R_{\dot{P}\dot{B}}$ amplitude and phase.

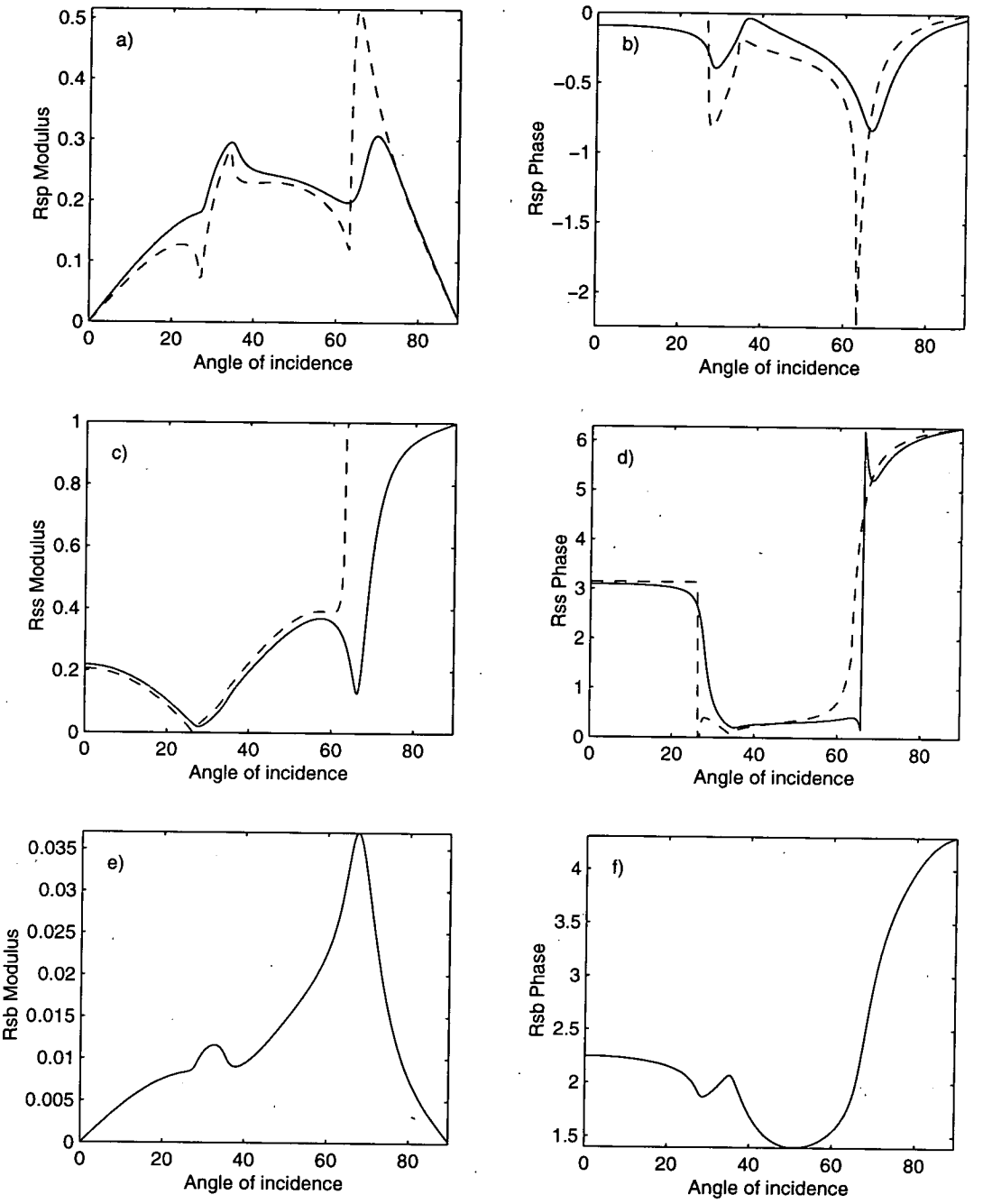

Figure 7.4. Dependence of reflection coefficients on the angle of incidence for poroelastic media at frequency $f = 32KHz$, S-wave incident. a) and b) $R_{\dot{S}\dot{P}}$ amplitude and phase. c) and d) $R_{\dot{S}\dot{S}}$ amplitude and phase. e) and f) $R_{\dot{S}\dot{B}}$ amplitude and phase.

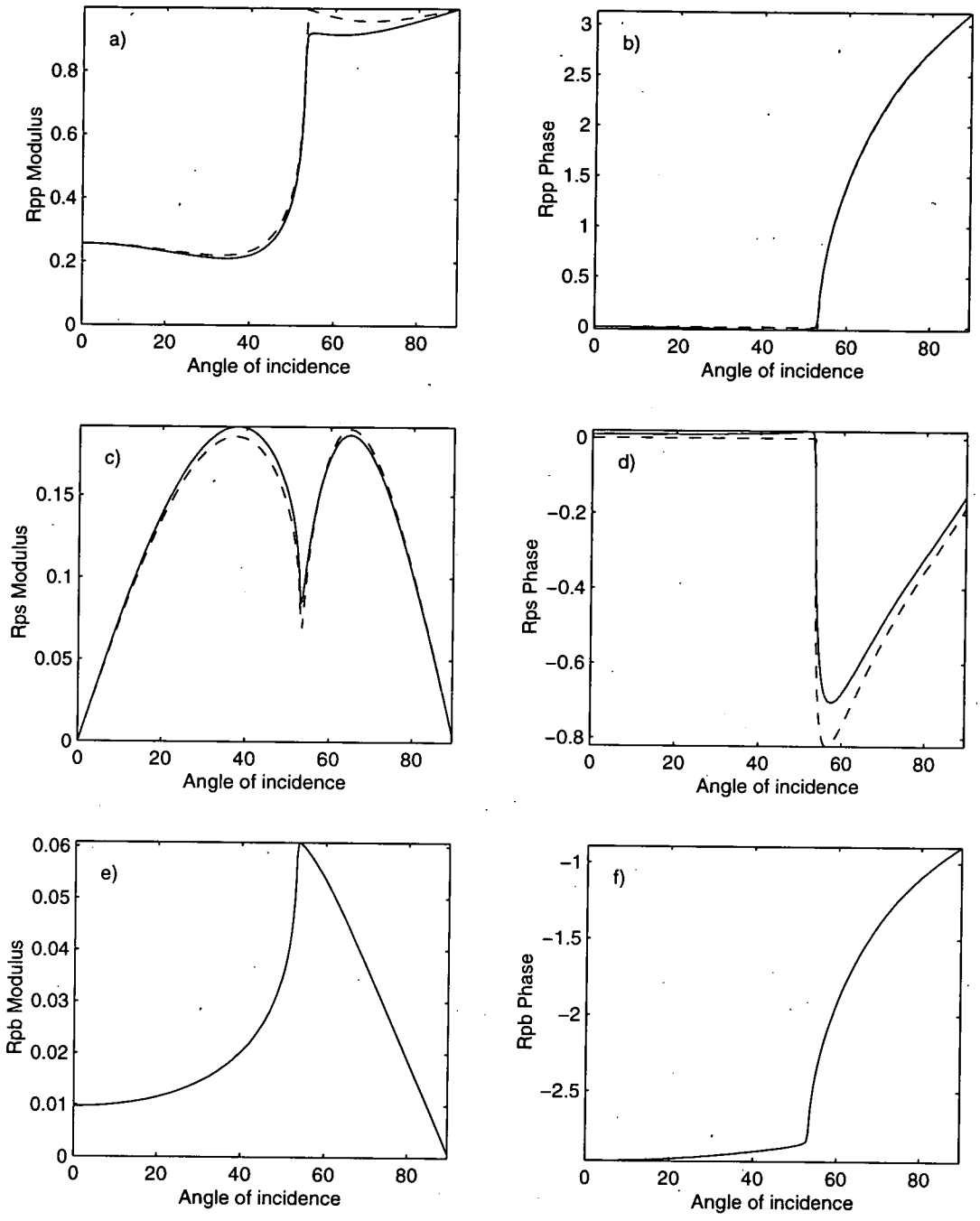

Figure 7.5. Dependence of reflection coefficients on the angle of incidence for poroelastic media at frequency $f = 64KHz$, P-wave incident. a) and b) $R_{\dot{P}\dot{P}}$ amplitude and phase. c) and d) $R_{\dot{P}\dot{S}}$ amplitude and phase. e) and f) $R_{\dot{P}\dot{B}}$ amplitude and phase. Solid curves: model for parameters in table 5.1.

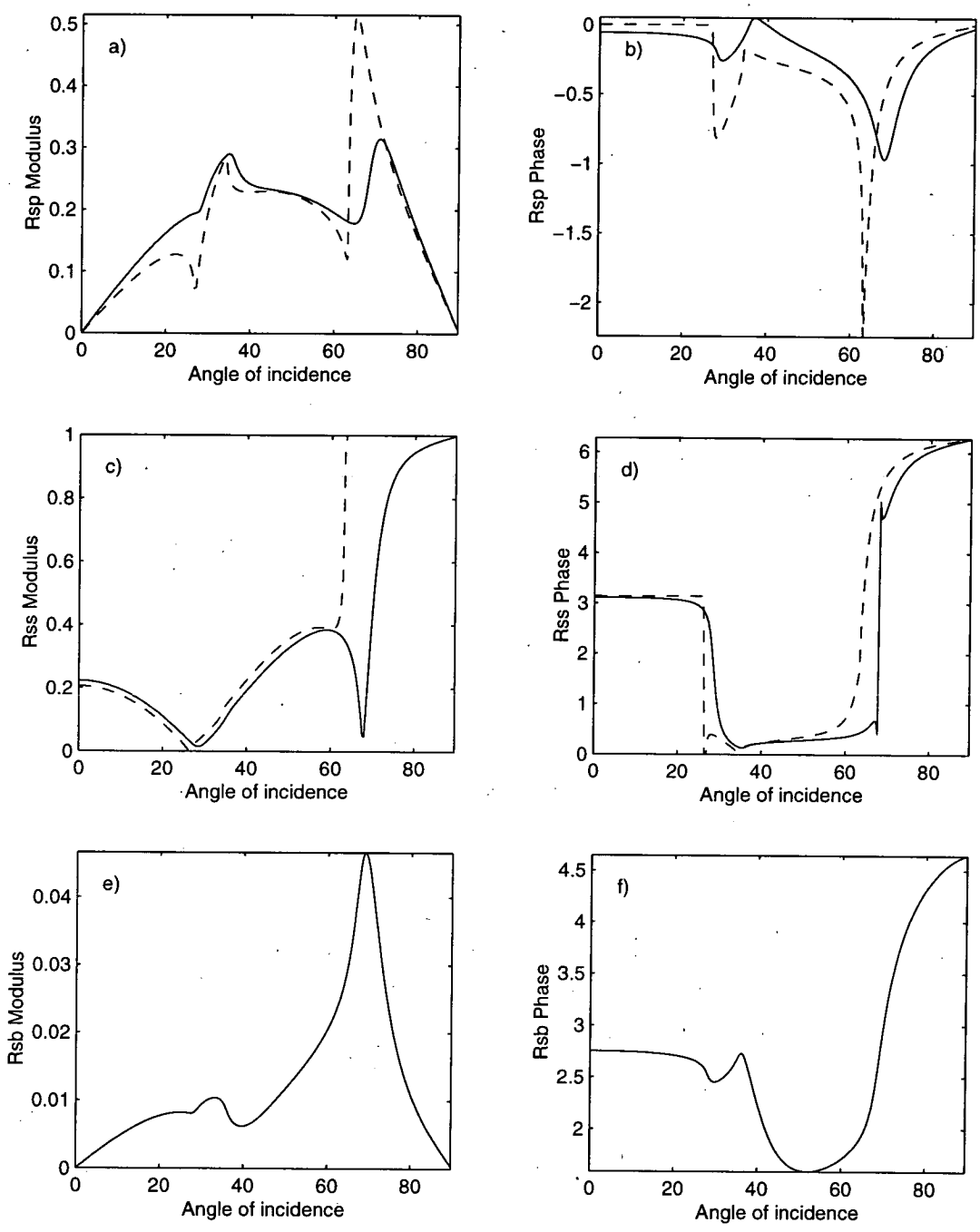

Figure 7.6. Dependence of reflection coefficients on the angle of incidence for poroelastic media at frequency $f = 64KHz$, S-wave incident. a) and b) $R_{\dot{S}\dot{P}}$ amplitude and phase. c) and d) $R_{\dot{S}\dot{S}}$ amplitude and phase. e) and f) $R_{\dot{S}\dot{B}}$ amplitude and phase. Solid curves: model for parameters in table 5.1.

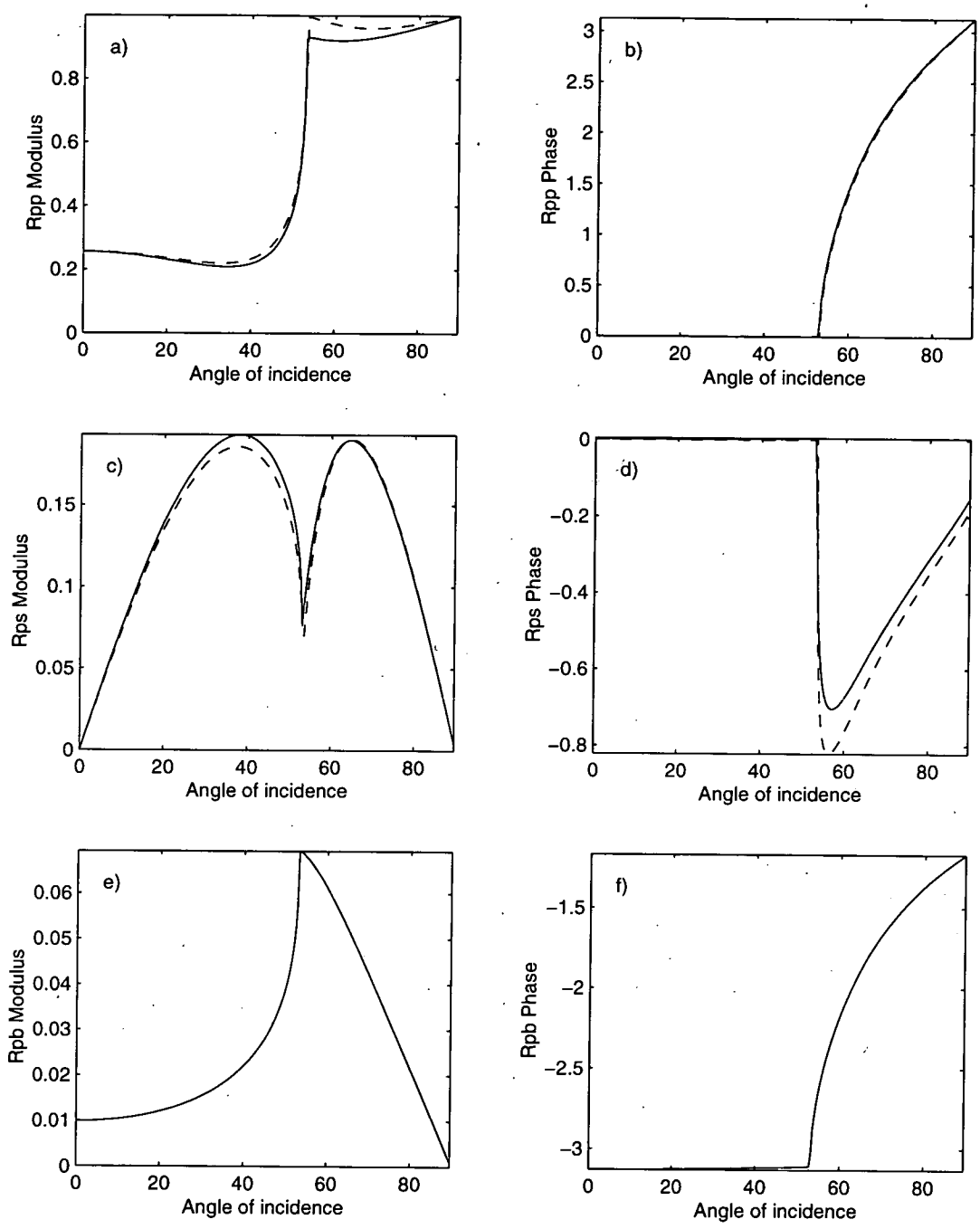

Figure 7.7. Dependence of reflection coefficients on the angle of incidence for poroelastic media at frequency $f = 640KHz$, P-wave incident. a) and b) $R_{\dot{P}\dot{P}}$ amplitude and phase. c) and d) $R_{\dot{P}\acute{S}}$ amplitude and phase. e) and f) $R_{\dot{P}\acute{B}}$ amplitude and phase. Solid curves: model for parameters in table 5.1.

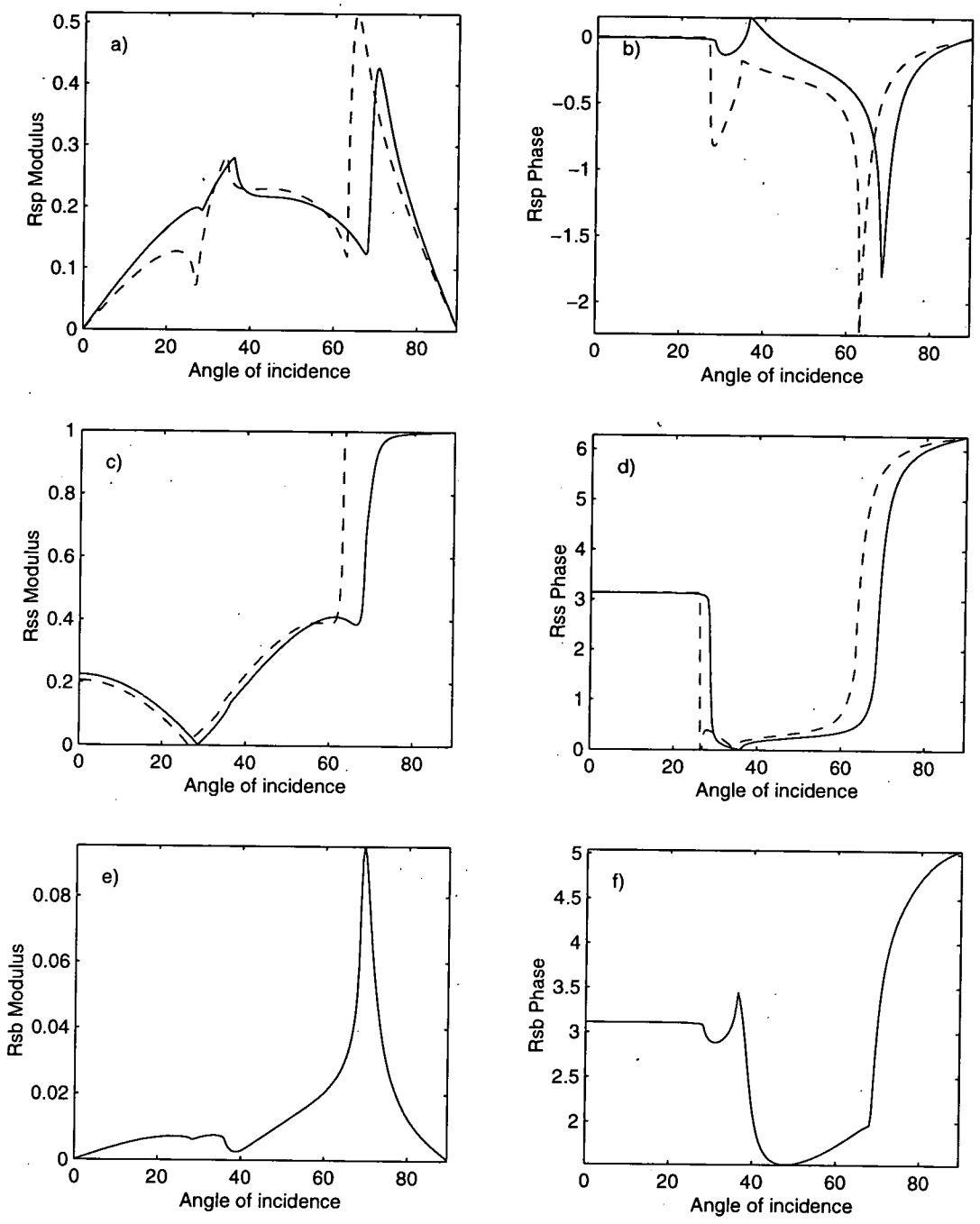

Figure 7.8. Dependence of reflection coefficients on the angle of incidence for poroelastic media at frequency $f = 640KHz$, S-wave incident. a) and b) $R_{\dot{S}\dot{P}}$ amplitude and phase. c) and d) $R_{\dot{S}\dot{S}}$ amplitude and phase. e) and f) $R_{\dot{S}\dot{B}}$ amplitude and phase. Solid curves: model for parameters in table 5.1.

7.3 Summary

Figures 7.1-7.8 show a steady increase with frequency of incident wave in the amplitude of the reflected Biot wave for R_{PB} and R_{SB} coefficients. Nevertheless, I observed no significant variations in R_{PP}, R_{PS}, R_{SP}, R_{SS} reflection coefficients for near normal angles of incidence. This means that the effect of Biot-wave at normal incidence is relatively small for the considered model of interface between two poroelastic media with petrophysical parameters given in table 7.1.

On the other hand, it can be clearly seen from figures 7.4, 7.6 and 7.8 that there is a pronounced effect of Biot-wave on reflected coefficients R_{SP} and R_{SS} near critical angles accompanied by strong changes in the phases of these coefficients. I suggest that this effect is caused by strong interaction between evanescent P- and/or S-wave with Biot wave at the interface. In the next chapter I look at the effect of frequency-dependence in more detail.

Chapter 8

APPLICATION TO OCEAN-BOTTOM SEDIMENTS

8.1 Introduction

In this chapter I investigate in more detail the effect of Biot-wave on reflection and transmission coefficients including reflection and transmission coefficients for energy flux.

I have choosen a model of interface between two unconsolidated ocean-bottom sediment layers (table 8.1) with higher porosities and permeabilities than in the model considered in the previous chapter. The higher values of porosity and permeability result in stronger influence of relative fluid flow in permeable matrix on seismic waves propagation and reflection coefficients. The numerical results show that in the unconsolidated ocean-bottom sediments up to 15% of incident seismic energy can be taken by the transmitted Biot-wave.

8.2 Numerical results

In this chapter I have decided to choose a purely poroelastic model without viscoelastic damping, i.e. log decrement $\delta = 0$. Consequently, all attenuation effects in this model are due to the relative viscous fluid flow i.e., caused by fluid viscosity. As in the previous chapter, I have two different characteristic Biot frequencies for top and bottom sediments: $\omega_B = 2.9\ 10^4$ for the top (mud) sediments and $\omega_B = 4.7\ 10^3$ for the bottom (sand) sediments. The parameters listed in table 8.1 are similar to typical parameters of ocean-bottom sediments [Stoll 1977].

Table 8.1

	Mud (top)	*Sand (bottom)*
K_r (GPa)	36.0	36.0
ρ_r $(g.cm^{-3})$	2.26	2.65
K_f (GPa)	2.0	2.0
ρ_f $(g.cm^{-3})$	1.0	1.0
η (cP)	0.01	0.01
K_b (GPa)	0.0121	1.38
μ (GPa)	0.0221	0.827
ϕ	0.76	0.47
c	1.25	1.25
k (cm^2)	$0.26\ 10^{-10}$	$0.1\ 10^{-5}$
δ	0.0	0.0
V_p $(Km.s^{-1})$	1.42	1.82
V_s $(Km.s^{-1})$	0.13	0.66
ω_B	$2.9\ \ 10^4$	$4.7\ 10^3$

I only consider here reflection and transmission coefficients caused by incident P-wave, which is a typical case for ocean-bottom sediments. Figure 8.1 shows the reflection and transmission coefficients for P-, S- and Biot-waves as a function of incident angle for three different frequencies: limiting case of zero-frequency, $100Hz$ and $1000Hz$. Figures 8.2 and 8.3 show the dependence of reflection and transmission coefficients including reflection and transmission coefficients for energy flux for normally incident P-wave. Figures 8.4 and 8.5 extend the results shown in figures 8.2 and 8.3 for different angles of incidence.

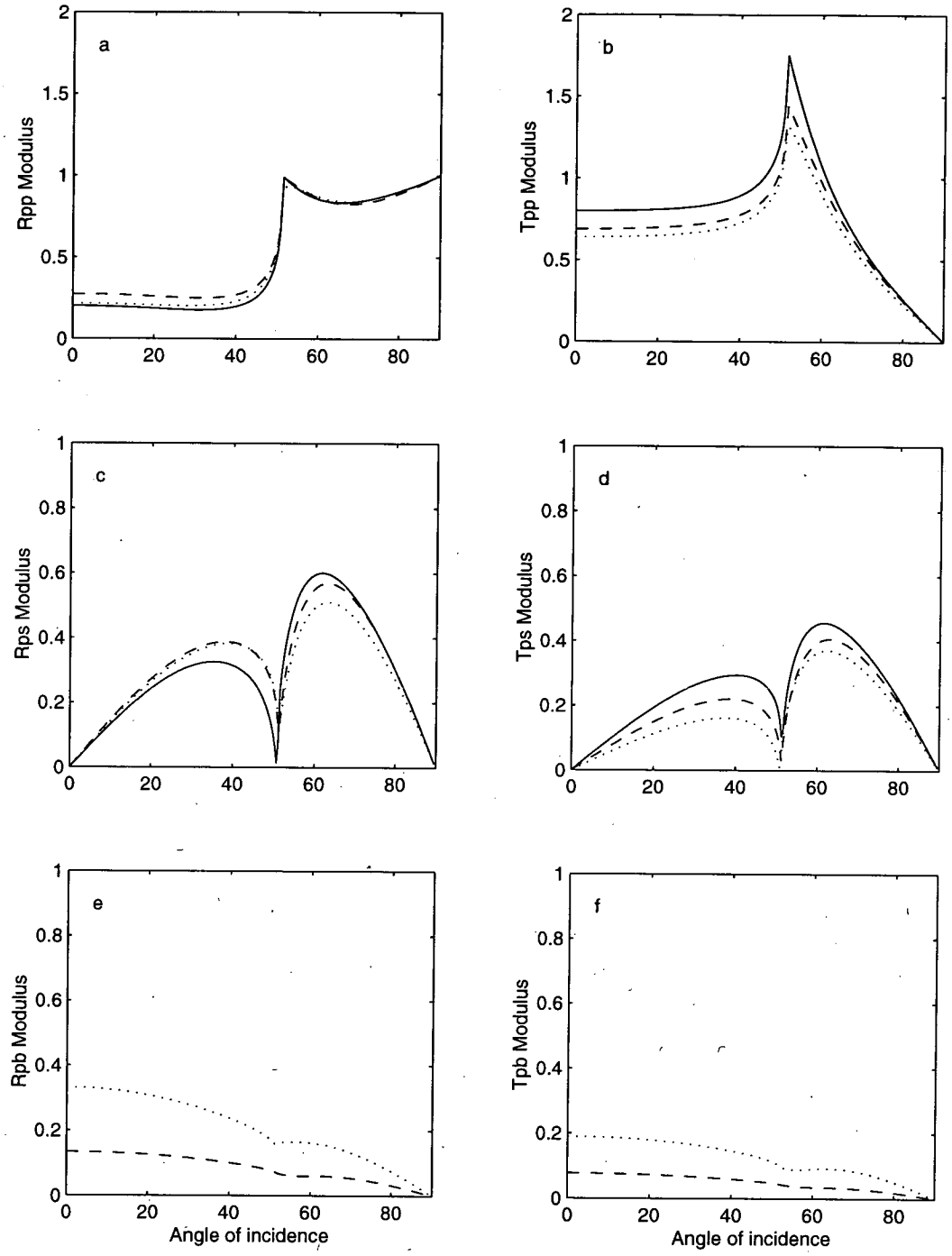

Figure 8.1. Dependence of amplitude RT coefficients on the angle of incident P-wave for mud over sand at different frequencies. a) $R_{\dot{P}\dot{P}}$ modulus. b) $T_{\dot{P}\dot{P}}$ modulus. c) $R_{\dot{P}\dot{S}}$ modulus. d) $T_{\dot{P}\dot{S}}$ modulus. e) $R_{\dot{P}\dot{B}}$ modulus. f) $T_{\dot{P}\dot{B}}$ modulus. Model: parameters for sediments are given in table (7.1), on top is mud, bottom is sand. Solid curves: elastic case. Dashed curves: 100Hz. Dotted curves: 1000Hz.

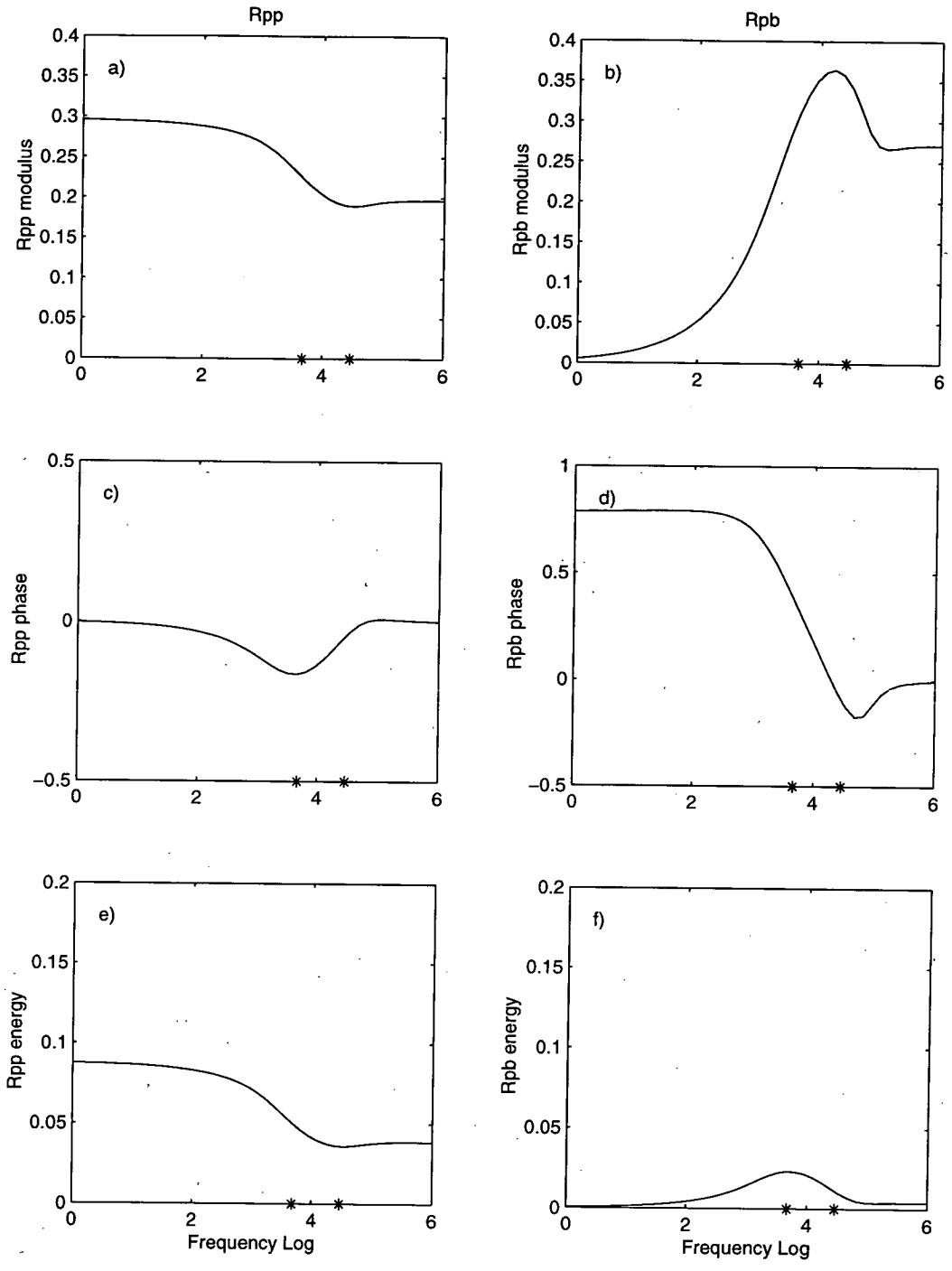

Figure 8.2. Frequency dependence of reflection coefficients, for mud over sand with P-wave at normal incidence. a) $R_{\dot{P}\dot{P}}$ modulus. b) $R_{\dot{P}\dot{B}}$ modulus. c) $R_{\dot{P}\dot{P}}$ phase. d) $R_{\dot{P}\dot{B}}$ phase. e) $\Re_{\dot{P}\dot{P}}$ coefficient. f) $\Re_{\dot{P}\dot{B}}$ coefficient. Model: parameters given in table (7.1), top medium is mud, bottom is sand. Stars on logarithmic frequencies axis are characteristic Biot frequencies.

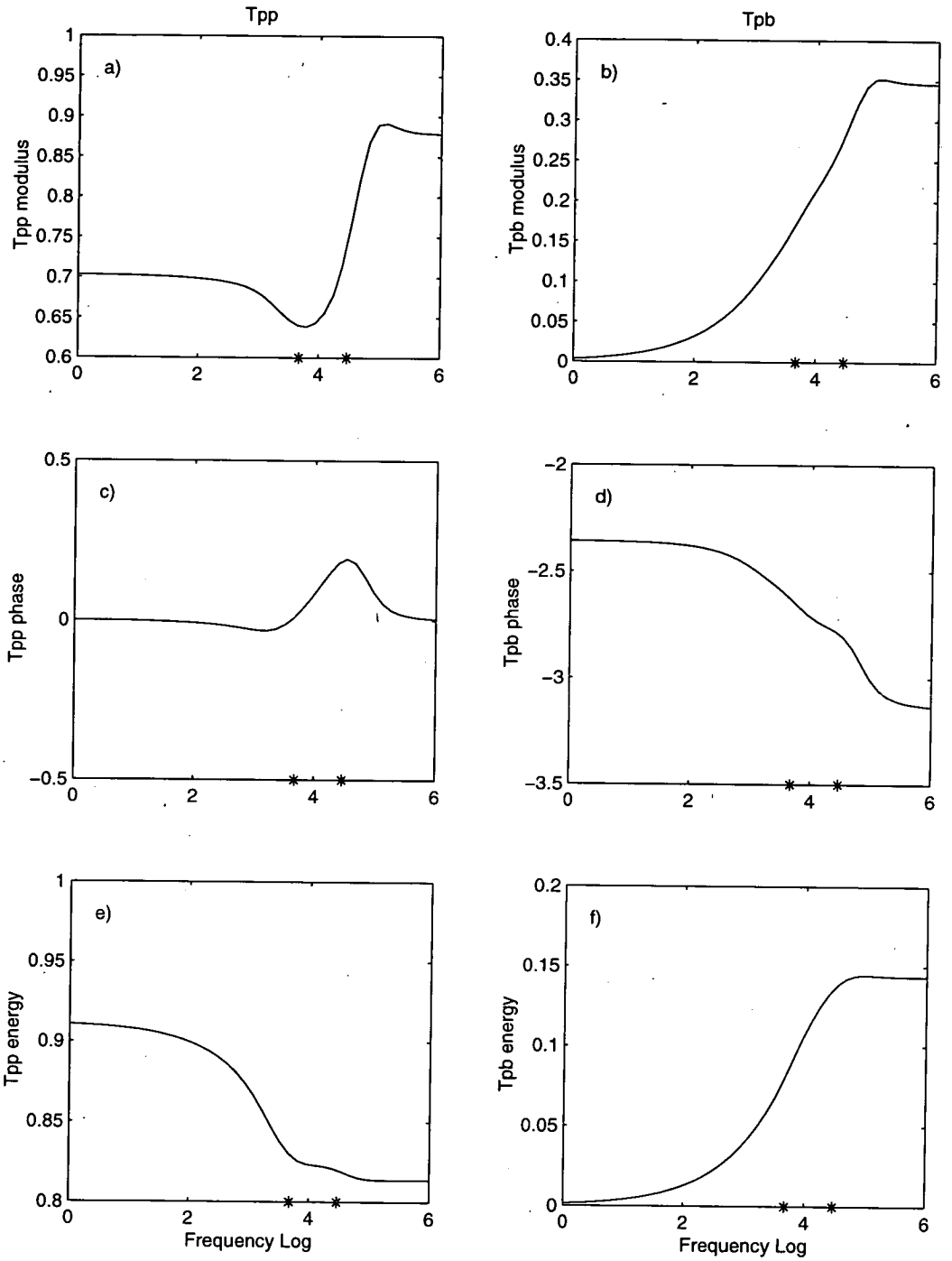

Figure 8.3. Frequency dependence of transmission coefficients, for mud over sand with P-wave at normal incidence. a) $T_{\dot{P}\acute{P}}$ modulus. b) $T_{\dot{P}\acute{B}}$ modulus. c) $T_{\dot{P}\acute{P}}$ phase. d) $T_{\dot{P}\acute{B}}$ phase. e) $\Im_{\dot{P}\acute{P}}$ coefficient. f) $\Im_{\dot{P}\acute{B}}$ coefficient. Model: parameters given in table (7.1), on top is mud, bottom is sand. Stars on logarithmic frequencies axis are characteristic Biot frequencies.

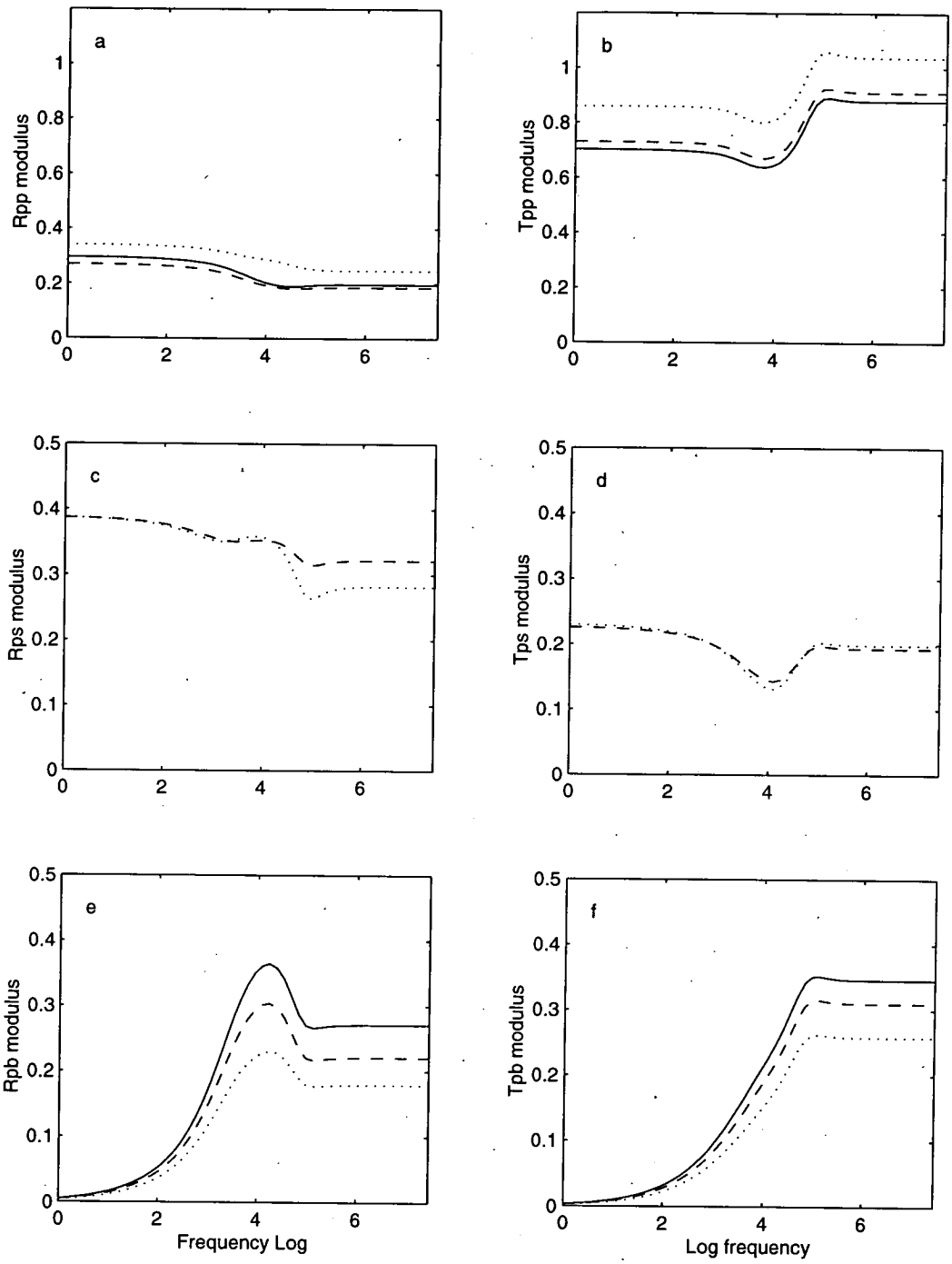

Figure 8.4. Frequency dependence of amplitude RT coefficients at different angles for mud over sand with P-wave incident. a) $R_{\grave{P}\acute{P}}$ modulus. b) $T_{\grave{P}\acute{P}}$ modulus. c) $R_{\grave{P}\acute{S}}$ modulus. d) $T_{\grave{P}\acute{S}}$ modulus. e) $R_{\grave{P}\acute{B}}$ modulus. f) $T_{\grave{P}\acute{B}}$ modulus. Model: parameters given in table (7.1), on top is mud, bottom is sand. Solid curves: normal incidence. Dashed curves: 15°. Dotted curves: 45°.

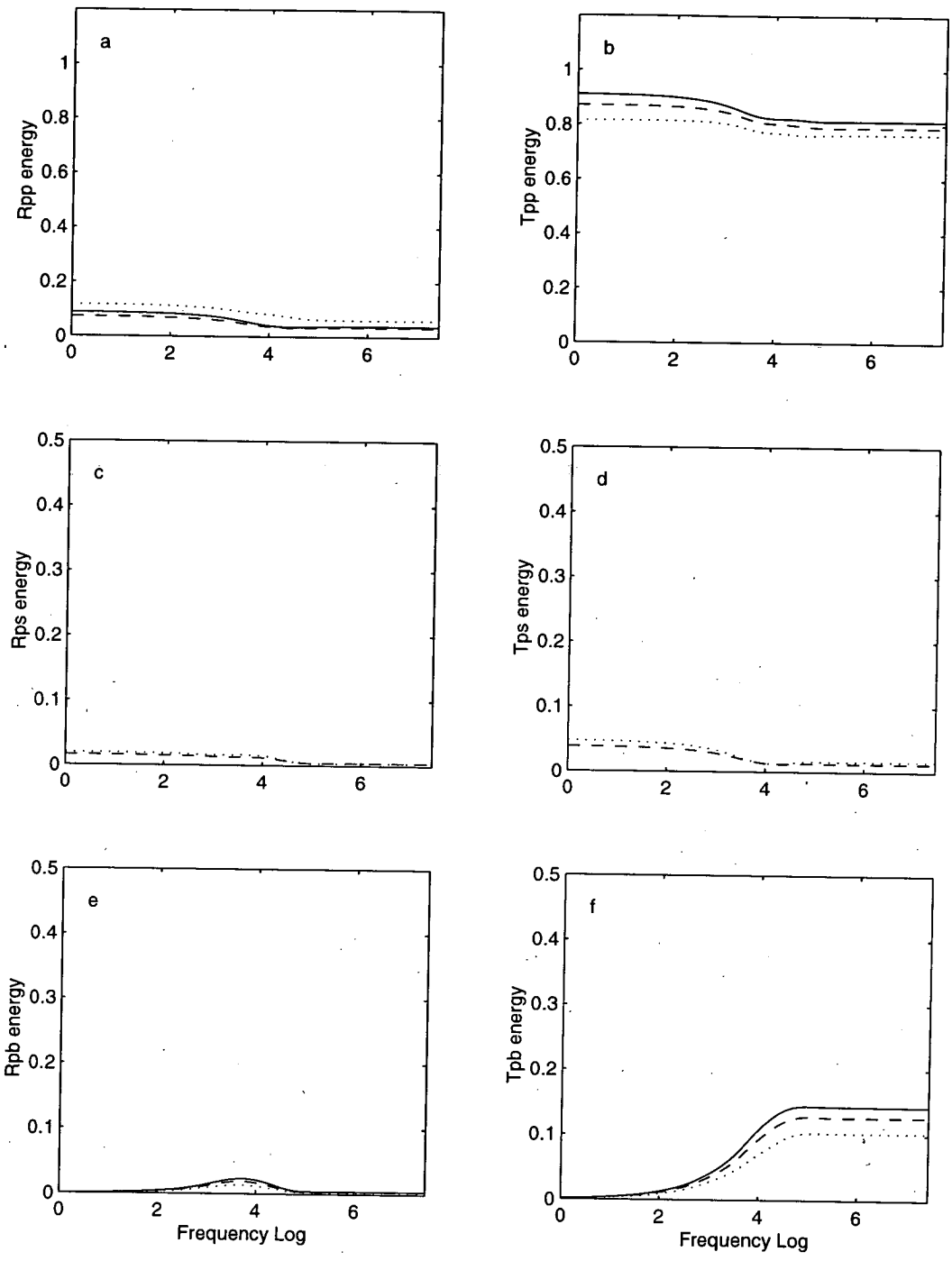

Figure 8.5. Frequency dependence of energy RT coefficients at different angles for mud over sand with P-wave incident. a) $\Re_{\dot{P}\acute{P}}$ coefficient. b) $\Im_{\dot{P}\acute{P}}$ coefficient. c) $\Re_{\dot{P}\acute{S}}$ coefficient. d) $\Im_{\dot{P}\acute{S}}$ coefficient. e) $\Re_{\dot{P}\acute{B}}$ coefficient. f) $\Im_{\dot{P}\acute{B}}$ coefficient. Model: parameters given in table (7.1), on top is mud, bottom is sand. Solid curve: normal incidence. Dashed curves: 15°. Dotted curve: 45°.

8.3 Summary

An overall impression from figures 8.1-8.5 is that the only region where Biot wave strongly effects reflections and transmissions of seismic waves is near or in-between the two Biot frequencies. That is certainly the case for the energy flux transmitted into the Biot-wave in the bottom layer. Figure 8.3 shows that up to 15% of energy is transmitted from the incident P-wave into the Biot wave. Interestingly enough only one or two percent of energy is taken by the reflected Biot-wave in the top (mud) layer (figure 8.5e). All moduli and phases of all reflection and transmission coefficients experienced strong variations in the vicinity of Biot frequencies.

At the low frequencies ($\omega < 2\pi \cdot 10^2$) and for near vertical incidence the effect of Biot wave is quite small if not negligible. Nevertheless, as we have discussed in the introduction, the situation can be quite different in the case of fine-layered fluid-saturated sediments. In this case an appropriate characteristic frequency is given by equation (1.2) of the introduction and this characteristic frequency can easily be inside the seismic range for fine-layered fluid-saturated sediments [White et al., 1975 and Pride et al. 2001]. It was first understood by White et al. [1975] that wave-induced fluid exchange between fine layers could have a strong influence on stratigraphic filtering.

Chapter 9

CONCLUSION

In this thesis I have considered Biot's theory for frequency-dependent wave propagation in fluid-saturated porous sediments. To link with petrophysical parameters of interest, I have used Stoll's formulation of Biot theory. This has led me to the work presented in this thesis: the derivation of reflection and transmission coefficients in fluid-saturated porous media. My main result is given by the matrix equations (5.15) and (5.24) for reflection and transmission coefficients at the interface between two fluid-saturated poroelastic half-spaces.

Following Biot [1956] I have derived dynamic equations of motion for porous elastic frame coupled with viscous pore-fluid. I have then derived wave equations for compressional and shear waves propagating in fluid-saturated poroelastic medium and the dispersion equations for plane harmonic waves. I have demonstrated that there are two compressional waves propagating in fluid-saturated permeable sediments. The second compressional wave (Biot wave) is a highly attenuating wave and was discovered by Maurice Biot in 1956. Despite relative insignificance of the effect of the *B*iot wave on *P*- and *S*-wave propagation in infinite homogeneous medium at seismic frequencies, it can affect reflection and transmission coefficients at the interface between highly permeable fluid-saturated sediments.

To address the problem of reflection and transmission of seismic waves in fluid-saturated porous medium, I have shown how to decompose seismic wave-fields into upgoing and downgoing components for all types of waves: *P*-wave, *B*iot wave, S_V and S_H waves. In doing this I have followed the approach developed by Taylor [1997]. These wave-field components are given explicitly in tables 4.1-4.4 and present one of the most important results of my thesis.

I have then discussed the problem of boundary conditions at the interface between poroelastic media and, following Deresiewicz and Skalak [1963], have introduced general boundary conditions at the horizontal interface between two fluid-saturated porous media. These boundary

conditions are given as eight continuity equations for the displacements and tractions in elastic frame and for pore-fluid velocity and pressure. Substituting the wave-field decomposition provided by tables 4.1-4.4 into the boundary conditions, I have derived matrix equations for reflection/transmission coefficients for all types of waves.

The matrix equation for S_H waves is decoupled from the reflection/transmission coefficients of all other waves and is given by equation (5.15). The main result however is given by matrix equation (5.24) coupling reflection and transmission coefficients for P-waves, Biot waves and S_V waves. The extended form of (5.24) is given by matrix equation (5.33) for the case when effect of partially sealed interface is taken into account. Matrix equations (5.15) for S_H-wave and (5.24) and (5.33) for P-,Biot and S_V-waves completely solve the reflection problem of plane harmonic waves in fluid-saturated poroelastic media.

I have then implemented my results in the form of a stable numerical algorithm for reflection, transmission and conversion coefficients valid for all frequencies and all angles of incidence. This algorithm depends on a set of petrophysical parameters proposed by Stoll [1977] for the description of permeable unconsolidated sediments. I have tested my algorithm in the appropriate (visco-)elastic limit with respect to the purely elastic model using a standard elastic algorithm for reflection and transmission coefficients [Aki and Richards 1980]. I have found an excellent agreement between my poroelastic algorithm and the purely elastic one even for a complicated model with two possible critical angles for an incident S_V-wave.

In the last two chapters I have demonstrated the effect of Biot wave on reflection and transmission of seismic waves at different frequencies and angles of incidence. My main conclusion is that a region where Biot wave strongly affects reflection and transmission of seismic waves is near or in-between the two Biot frequencies (the characteristic frequencies of top and bottom sediment layers) and in the vicinity of critical angle(s). The reason for the latter is, presumably, a strong interaction between Biot wave and evanescent P- or S-waves.

The numerical results for unconsolidated highly permeable ocean-bottom sediments demonstrate that up to 15% of energy goes from the incident P-wave into the transmitted Biot wave. Interestingly enough, only one or two percent of energy is taken by the reflected Biot-wave. This is probably due to a higher value of specific permeability in the bottom layer sediments (coarse sand). All moduli and phases of all reflection and transmission coefficients experience strong variations in the vicinity of Biot frequencies.

At low frequencies and for near vertical incidence the effect of Biot wave is quite small if not

negligible. Nevertheless, as we discussed in the introduction, the situation can be quite different in the case of fine-layered fluid-saturated sediments. In this case an appropriate characteristic frequency is given by equation (1.2) of the introduction and this frequency can easily be inside seismic range for fine-layered fluid-saturated sediments [Pride et al. 2001]. It was first understood by White et al. (1975) that wave-induced fluid exchange between fine layers could have a strong influence on stratigraphic filtering.

There is a range of possible applications of my algorithm, and the seismic-filtering problem is only one of them. It is rather obvious that the interpretation of reflection, transmission and conversion (RTC) coefficients in fluid-saturated sediments is of utmost importance for the characterisation of hydrocarbon reservoirs.

It has also been suggested that high-pressure pore-fluid is responsible for anomalously high (up to 0.15-0.25) values of reflection coefficients (deep crustal reflectors) in the lower crust and subduction zones [Meissner 1986]. Several different mechanisms have been suggested to explain high values of reflection coefficients in the lower crust but the problem still remains unresolved.

Another quite unexpected possible application of my algorithm is related to the problem of global warming. It has been discovered that part of the West Antarctic ice sheet is underlain by a thin layer of deforming water-soaked sediments [Boulton 1986]. In such areas the rheological instability of subglacial sediments must largely control the dynamic behaviour of the whole ice sheet. Seismic reflection surveys were undertaken in recent years to identify the location of unstable sediments with high pore-water pressure under the ice sheet. The correct interpretation of reflection coefficients observed in these field experiments is possible only in the frame of the poroelastic theory.

References

Aki K. and Richards P.G. (1980). Quantitative seismology. W.H. Freeman and Company.

Backus G.E. (1962). *Long-wave elastic anisotropy produced by horizontal layering*, J. of Geophysical Research, 67, pp 4427-4440.

Biot M.A. (1956a). *Theory of propagation of elastic waves in a fluid-saturated porous solid.* J. Acoust. Soc. Am., 28, pp 168-191.

Biot M.A. (1962). *Mechanics of deformation and acoustic propagation in porous media.* J. Appl. Phys., 33, pp 482-1498.

Boulton G.S. (1986). *A paradigm shift in glaciology?* Nature, 322, p18.

Bourbié T. , Coussy O. and Zinszner B. (1986). *Acoustique des milieux poreux.* Editions Technip.

Bourbié T. ; Gonzales-Serrano A. (1983). *Synthetics seismograms in attenuating media.* Geophysics, 48, pp 575-1587.

Carcione J.M., Kosloff D. and Behle A. (1991). *Long-wave anisotropy in stratified media : A numerical test*, Geophysics, vol 56, pp 245-254.

Crampin S., Taylor D.B. (1998). *Effects of poorly-consolidated sediments on seafloor seismograms.* Processing 3-component seafloor seismic data; Semi-annual report 4. University of Edinburgh.

Cruz V. de la, Spanos T.J.T. (1985). *Seismic wave propagation in a porous medium.* Geophysics, 50, pp 1556-1565.

Dautray R. and Lions J.-L. (1984). *Analyse mathematique et calcul numerique pour les sciences et les techniques.* Masson S.A.

Deresiewicz H. and Rice J.T. (1962). *The effect of boundaries on wave propagation in a liquid-*

filled porous solid: III. Reflection of plane waves at a free plane boundary (general case). Bull. Seismol. Soc. Am., 52, pp 595-625.

Deresiewicz H. and Rice J.T. (1964). *The effect of boundaries on wave propagation in a liquid-filled porous solid: V. Transmission across a plane interface.* Bull. Seismol. Soc. Am., 54, pp 409-416.

Deresiewicz H. and Skalak R. (1963). *On uniqueness in dynamic poroelasticity.* Bull. Seismol. Soc. Am., 53, pp 783-788.

Dvorkin J. and Nur A. (1993). *Dynamic poroelasticity: A unified model with the squirt and Biot mechanisms*, Geophysics, vol 58, pp 524-533.

Gassmann F. (1951). *Uber die Elastizitat poroser Medien.* Vier. der Natur. Gesellschaft in Zurich, 96, pp1-23.

Geertsma J. and Smit D.C. (1961). *Some aspects of elastic wave propagation in fluid-saturated porous solids.* Geophysics, 26, pp 169-181.

Gelinsky S., Shapiro S.A. (1997). *Dynamic equivalent-medium approach for thinly layered saturated sediments.* Geophys. J. Int., 128, F1-F4.

Graebner M. (1992). *Plane-wave reflection and transmission coefficients for a transversely isotropic solid.* Geophysics, 57, pp 1512-1519.

Gurevitch B. (1996). *Numerical simulations of ultrasonic experiments on poroelastic samples.* EAGE Expanded Abstract, C032.

Gurevitch B. and Lopatnikov S.L. (1995). *Velocity and attenuation of elastic waves in finely-layered porous rocks.* Geophys. J. Int., 121, pp 933-947.

Gurevitch B. and Schoenberg M. (1999). *Interface conditions for Biot's equations of poroelasticity.* J. Acoust. Soc. Am., 105 (5), pp 2585-2589.

Hajra S. and Mukhopadhyay A. (1982).*Reflection and refraction of seismic waves incident obliquely at the boundary of a liquid-saturated porous solid.* Bull. Seismol. Soc. Am. 72, pp 1509-1533.

Helbig K. (1984). *Anisotropy and dispersion in periodically layered media.* Geophysics, 49, pp 364-373.

Hudson J.A. (1962). *The total internal reflection of SH waves.* Geophys. J. of Royal Acad. Soc., 6, pp 509-531.

Hudson J.A. and Knopoff L. (1989). *Predicting the overall properties of composites - materials with small-scale inclusions of cracks.* Pure Appl. Geophys., 131, pp 551-576.

Kennett B.L.N. (1983). *Seismic wave propagation in stratified media.* Cambridge University Press.

Lee C.C., Lahham C.C., Martin B.G. (1990). IEEE Transactions on ultrasonics, ferroelectrics and frequency control, 37(4).

Levy Th. and Sanchez-Palencia E. (1977). *Equations and interface conditions for acoustic phenomena in porous media.* J. of Math. Analysis and applications, 61, pp 813-834.

Meissner R. (1986). The continental crust, a geophysical approach. International Geophysics Series (34). Academic Press.

Mukerji T., Mavko G., Mujica D and Lucet N. (1995). *Scale-dependent seismic velocity in heterogeneous media.* Geophysics 60, pp 1222-1233 .

O'Doherty R.F. and Anstey N.A. (1971). *Reflections on amplitudes.* Geophys. Prosp., 19, pp 430-458.

O'Donnell M., Jaynes E.T. and Miller J.G. (1978). *General relationships between ultrasonic attenuation and dispersion.* J. Acoust. Soc. Am. 63, pp 1935-1937.

Plona T.J. (1980). *Observation of a second bulk compressional wave in a porous medium at ultrasonic frequencies.* Appl. Phys. Lett. 19, pp 548-553.

Pride S.R., Tromeur E. and Berryman J.G. (2001). *Biot slow-wave effects in stratified rock.* Geophysics online.

Rasolofosaon P.N.J. (1988). *Importance of the interface hydraulic condition on the generation of second bulk compressional wave in porous media.* Appl. Phys. Lett. 52, pp 780-782.

Rasolofosaon P.N.J. (1991). *Plane acoustic waves in linear viscoelastic porous media: Energy, particle displacement, and physical interpretation.* J. Acoust. Soc. Am. 89, pp1532-1550.

Rosenbaum J.H. (1974). *Synthetic seismograms: logging in porous formations.* Geophysics 39, pp 14-32.

Sams M.S. (1995). *Attenuation and anisotropy : The effect of extra fine layering.* Geophysics, 60, pp 1646-1655.

Schoenberg M. (1985). *Transversely isotropic media equivalent to thin isotropic layers.* Geophysical Prospecting, 42, pp 885-915.

Schoenberg M. and Muir F. (1989). *A calculus for finely layered anisotropic media.* Geophysics, 54, pp 581-589.

Stoll R. (1977). *Acoustic waves in ocean sediments* Geophysics, 42, pp715-725.

Stoll R. (1989). *Sedimentary Acoustics.* Lecture notes in Earth Sciences (26), Springer-Verlag.

Taylor D.B. (1997). *Implementation of Stoll-Biot-mud in ANISEIS.* Processing 3-component seafloor seismic data; Semi-annual report 3. University of Edinburgh.

Thompson A.H., Katz A.J. and Krohn C.E. (1987). *The microgeometry and transport properties of sedimentary rock.* Advances in Physics, 36, pp 625-694.

Vries S.M. de (1989). *Propagation of transient acoustic waves in porous media.* PhD thesis, Delft University of technology.

White J.E., Mikhaylova N.G. and Lyakhovitsky F.M. (1975). *Low-frequency seismic waves in fluid-saturated layered rocks.* Izvestija Academy of Sciences USSR, Phys. Solid Earth, 11, pp 654-658.